Doctor of Philosophy

The study for molecular mechanisms of erastin-induced ferroptosis

The Graduate school of the University of Ulsan

Department of Biological science

Eunhee Park

The study for molecular mechanisms of erastin-induced ferroptosis

Supervisor: Professor Su Wol Chung, Ph.D

A Dissertation

Submitted to
The Graduate Schhol of the University of Ulsan
In partial Fulfillment of the Requirements
for the degree of

Doctor of Philosophy

By

Eunhee Park

Department of Biological Science
Ulsan, Korea
February 2021

The study for molecular mechanisms
of erastin-induced ferroptosis

This certifies that the dissertation
of Eunhee Park is approved by

Committee Chair Dr. SUNG HOON BACK

Committee Member Dr. HONG PYO KIM

Committee Member Dr. HYE SEON CHOI

Committee Member Dr. JEONG-WOO PARK

Committee Member Dr. SU WOL CHUNG

Department of Biological Science
Ulsan, Korea.
February 2021

Contents

Overview

The mechanism and regulation

of ferroptosis

Abbreviations

ROS	Reactive oxygen species
RCD	Regulated cell death
GSH	Glutathione
GPX4	Glutathione peroxidase 4
NADPH	Nicotinamide adenine dinucleotide phosphate
MAPK	Mitogen-activated protein kinase
DFO	Deferoxamine
TfR	Transferrin receptor
DMT1	Divalent metal transporter 1
FTL	Ferritin light chain
FTH1	Ferritin heavy chain 1
PUFAs	Polyunsaturated fatty acids
ACSL4	Acyl-coA synthetase long-chain

Introduction

1. Ferroptosis

1.1 Discovery of ferroptosis

Ferroptosis is a type of regulated cell death dependent on iron and reactive oxygen species (ROS), and is characterized by lipid peroxidation [1]. Ferroptosis was originally observed when screening small molecule compounds for targeting oncogenic RAS mutations. This screen led to the identification of a small molecule compound termed 'erastin' that selectively kill genetically-engineered cells with an oncogenic RAS mutation [2]. In 2012, Stockwell et al. finally describe erastin-induced cell death as an iron-dependent RCD that was called 'ferroptosis' [2]. Erastin-induced iron accumulation promotes reactive oxygen species (ROS) production, which results in lipid peroxidation and subsequent death. Erastin induced cell death can be avoided by iron chelation or antioxidants [3]. Later, other chemical compounds, including sulfasalazine, RSL3, sorafenib, artemisinins, and five-membered ring cyclic peroxide 1, 2-dioxolane (FINO2), were confirmed to have the capacity for induce ferroptosis [4] (Figure 1).

1.2 The features of ferroptosis

Ferroptosis differs from other forms of regulated cell death such as apoptosis and necrosis in morphological, biochemical, and genetic levels [4] (Figure 2). Morphological changes during apoptosis include chromosome shrinkage, chromatin condensation, peripheralization, and round or oval cytoplasmic fragment formation [5], whereas ferroptosis is characterized by cell swelling and mitochondria become smaller, with increased mitochondria membrane densities, reduced mitochondria crista [6]. At a structural level, ferroptotic cells show altered mitochondrial morphology including electron-dense mitochondria and outer-membrane rupture [6]. In the biochemically, apoptosis include

inter-nucleosomal DNA fragment, caspase activation [7], whereas ferroptotic cells inhibition of system Xc^- and reduced GSH, inhibition of GPX4, and increased Fe, ROS and lipid peroxidation [6].

1.3 The regulators and mechanisms of ferroptosis

Iron and ROS accumulation, inhibition of system Xc^- with decreased cystine uptake, GSH depletion, increased NADPH oxidation and activation of MAPKs are central biochemical events leading to ferroptosis [6, 9]. Iron is an important trace nutrient in human, but excessive iron can cause tissue injury and increase the risk of developing cancers [9, 10]. Transferrin is the major iron transport protein. Fe^{3+} is the form of iron that binds to transferrin, so the Fe^{2+} transported through ferroportin must be oxidized to Fe^{3+} [11]. Iron-transferrin complex binds to the cell-surface transferrin receptor (TfR) 1, resulting in endocytosis and uptake of the metal cargo and then locates in the endosome. In the endosome, Fe^{3+} is reduced to ferrous iron (Fe^{2+}) by the ferrireductase activity. Finally, divalent metal transporter 1 (DMT1) mediates the release of Fe^{2+} from the endosome into a labile iron pool in the cytoplasm [12]. Excess iron is stored in ferritin, an iron storage protein complex including ferritin light chain (FTL) and ferritin heavy chain 1 (FTH1) [14]. Increased iron uptake and reduced iron storage can result in an iron overload during ferroptosis [14]. Genetic manipulations of iron metabolism pathways affect ferroptosis sensitivity. Excessive iron contributes to ferroptosis through generating toxic ROS [15]. Endogenous antioxidants such as superoxide dismutase, glutathione (GSH), and catalase can protect the cell from ROS damage [16]. Imbalance in the rate of ROS generation and detoxification leads to oxidative stress and can damage DNA, proteins and lipids [17]. ROS can react with the polyunsaturated fatty acids (PUFAs) in lipid membranes to induce lipid peroxidation. PUFAs are oxidized by both enzymatic and non-enzymatic pathways [18]. In addition to non-enzymatic free-radical chain reactions, the activation of the lipoxygenase-dependent enzymatic pathway involving ACSL4 (acyl-coA synthetase long-chain) family member and LPCAT3 (lysophosphatidylcholine acyltransferase) plays a key role in the generation of lipid hydroperoxides from PUFAs during ferroptosis [19]. The role of antioxidant events has also received widespread attention in the process of ferroptotic cancer cell death. GPX4, is an

antioxidant enzyme that neutralizes lipid peroxides and protects membrane fluidity. It uses glutathione as a cofactor to catalyze the reduction of lipid peroxides and protects cells and membranes against peroxidation [18]. Inhibition of GPX4 initiates uncontrolled polyunsaturated fatty acid (PUFA) oxidation and fatty acid radical generation thereby causing ferroptotic cell death [20]. Intracellular levels of glutathione (GSH), a cofactor of GPX4, are also influenced by the function of the system Xc^- SLC7A11 cystine-glutamate antiporter. By suppressing system Xc^- to prevent extracellular cysteine from uptaking into cells and to reduce the intracellular GSH level, erastin results in iron-dependent cell death mediated by the accumulation of lipid peroxidation [4]. System Xc^- maintains the production of GSH through serial reactions after exchanging extracellular cystine and intracellular glutamate. GSH depletion resulting from system Xc^- inhibition is implicated in various human diseases, especially central nervous system disorders. Inhibiting system Xc^- can trigger ferroptosis, whereas increasing cystine uptake into cells inhibits erastin-induced ferroptosis [21] (Figure 3).

1.4 Ferroptosis in cancer

Programmed cell death is a hot topic both in biological research and medicine (Figure 4). A common way of cancer treatment is to target the cell death process. (Figure 5). Ferroptosis, as a new coined programmed cell death process is characterized with unique features and shows great potentials in the cancer treatment [22]. The anticancer activity of erastin was tested in 117 cancer cells [23]. Diverse cancer cells, such as breast cancer cells, HCC, pancreatic cancer cells, cervical carcinoma, osteosarcoma and prostate adenocarcinoma cells, are very susceptible to ferroptosis. Various studies have confirmed the pivotal role of ferroptosis in killing cancer cells and suppressing tumour growth. Besides exerting single effects, erastin also enhances chemotherapy drugs such as temozolomide, cisplatin, and doxorubicin in certain cancer cells [6]. However, the roles of ferroptosis in cancer development, progression and treatment remains clear.

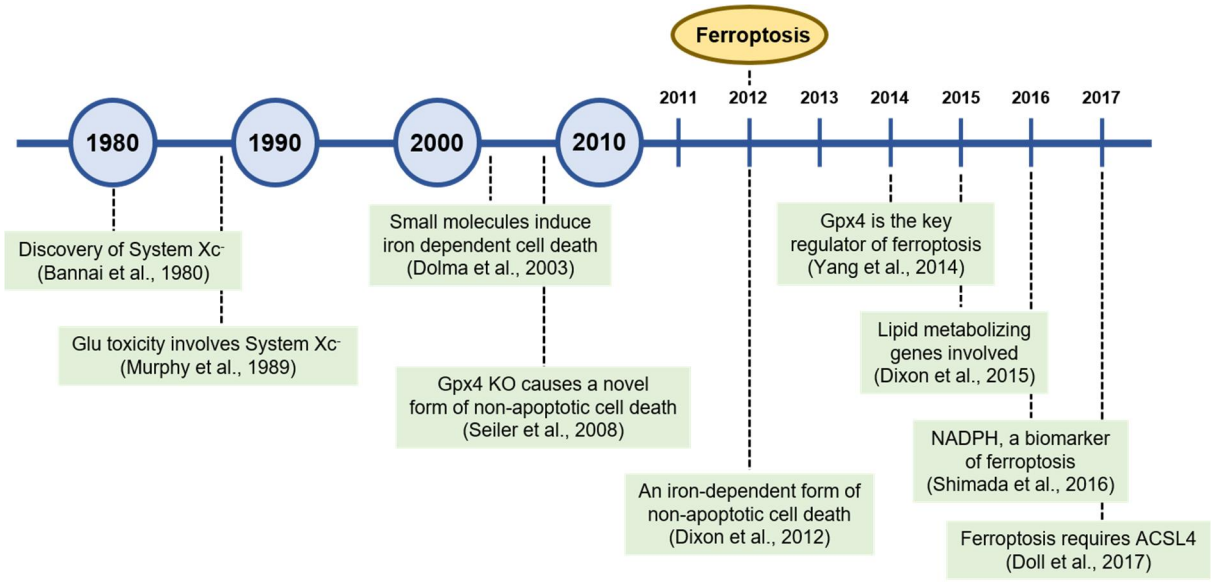

Figure 1. Schematic timeline depicting important discoveries in the field of ferroptosis research

Schematic timeline highlights key discoveries that contributed to the emergence of the concept of ferroptosis and important observations that are consistent with the current definition of ferroptosis, before it ferroptosis termed. This figure was modified from *IUBMB Life*. 2017 Jun;69(6):423-434.

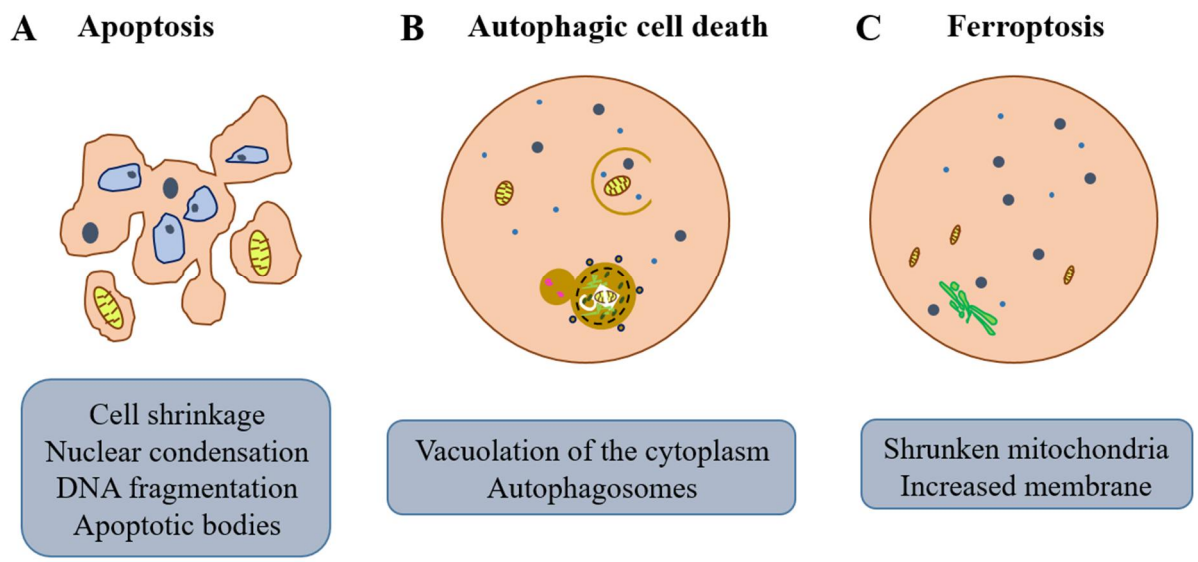

Figure 2. Morphology of apoptosis, autophagic cell death, and ferroptosis

The characteristics of each subroutine such as apoptosis (A), autophagic cell death (B), and ferroptosis (C) are summarized in the box below. Apoptosis, also namely type I PCD, is an evolutionarily conserved cell suicide mechanism in order to eliminate redundant, damaged, or infected cells. Macroautophagy (hereafter referred as autophagy) is a highly conserved cellular self-digestion process by which cellular components are targeted to lysosomes for their degradation. In morphology, double membrane containing vesicles that engulf cellular components, called autophagosomes can be observed. Ferroptosis is a type of iron-dependent cell death that first reported in 2012, whose morphologic features include smaller mitochondria and increased membrane density. This figure was modified from *Med Res Rev*. 2016 Nov;36(6):983-1035.

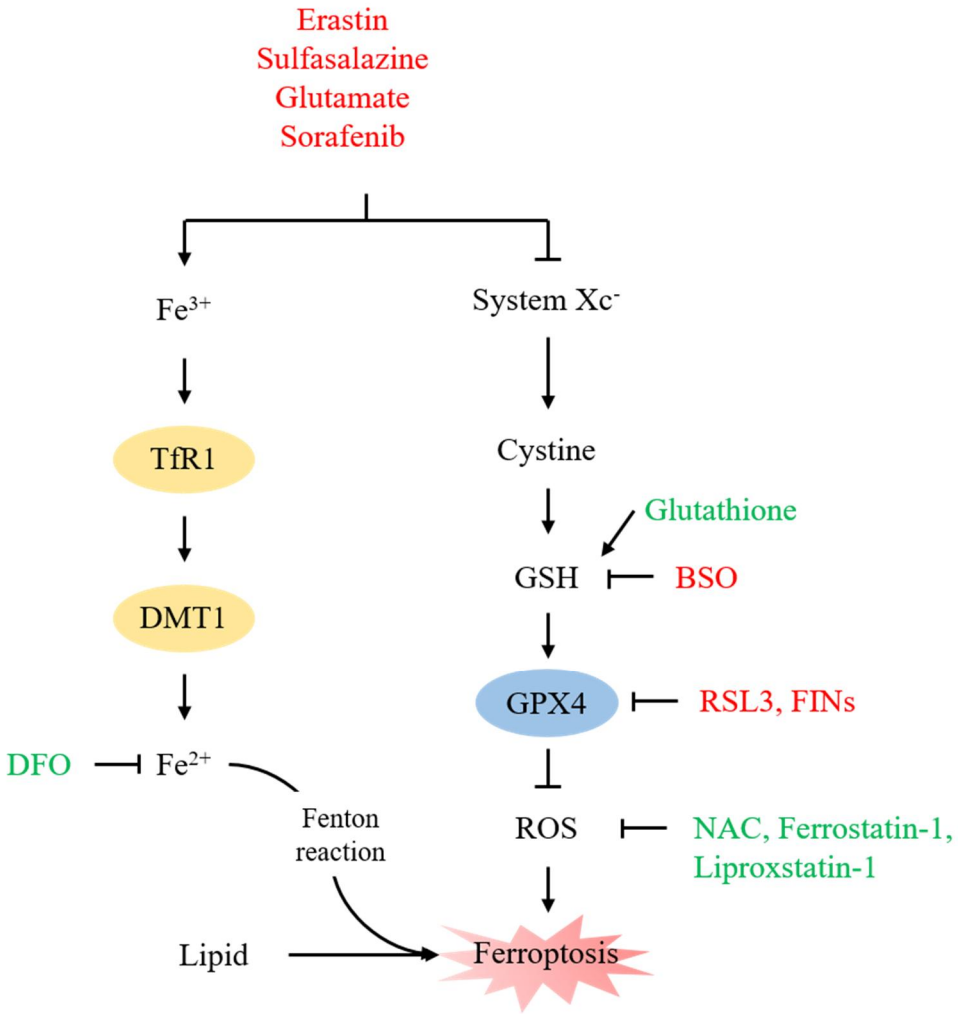

Figure 3. Molecular mechanisms and signaling pathways of ferroptosis.

Ferroptosis is initiated by the inhibition of system Xc^- or GPX4 activity, which ultimately leads to cell death. Lipid ROS maybe responsible for the ferroptotic process. On the one hand, the lipid peroxidation is considered to be an important contributor. On the other hand, excess irons are the basis for ferroptosis execution. This figure was modified from Cell *Death & Differentiation* 2016. 23, 369–379.

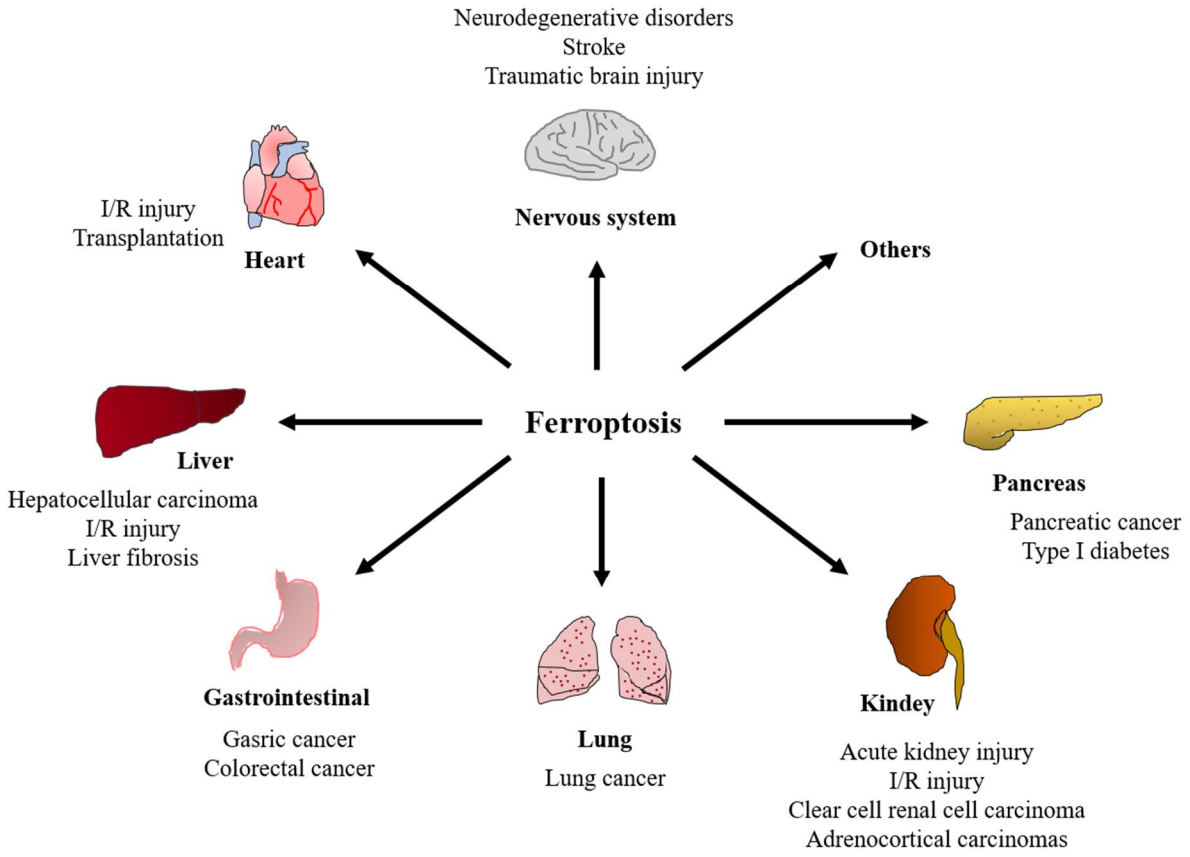

Figure 4. Ferroptosis has played important roles in multiple system diseases

Ferroptosis plays an important regulatory role in the occurrence and development of many diseases and has become the focus and hotspot of research on the treatment and prognosis improvement of related diseases. Recent studies have shown that ferroptosis plays an important regulatory role in the occurrence and development of many diseases and has become the focus and hotspot of research on the treatment and prognosis improvement of related diseases. This figure was modified from *Cell Death Dis*. 2020 Feb 3;11(2):88.

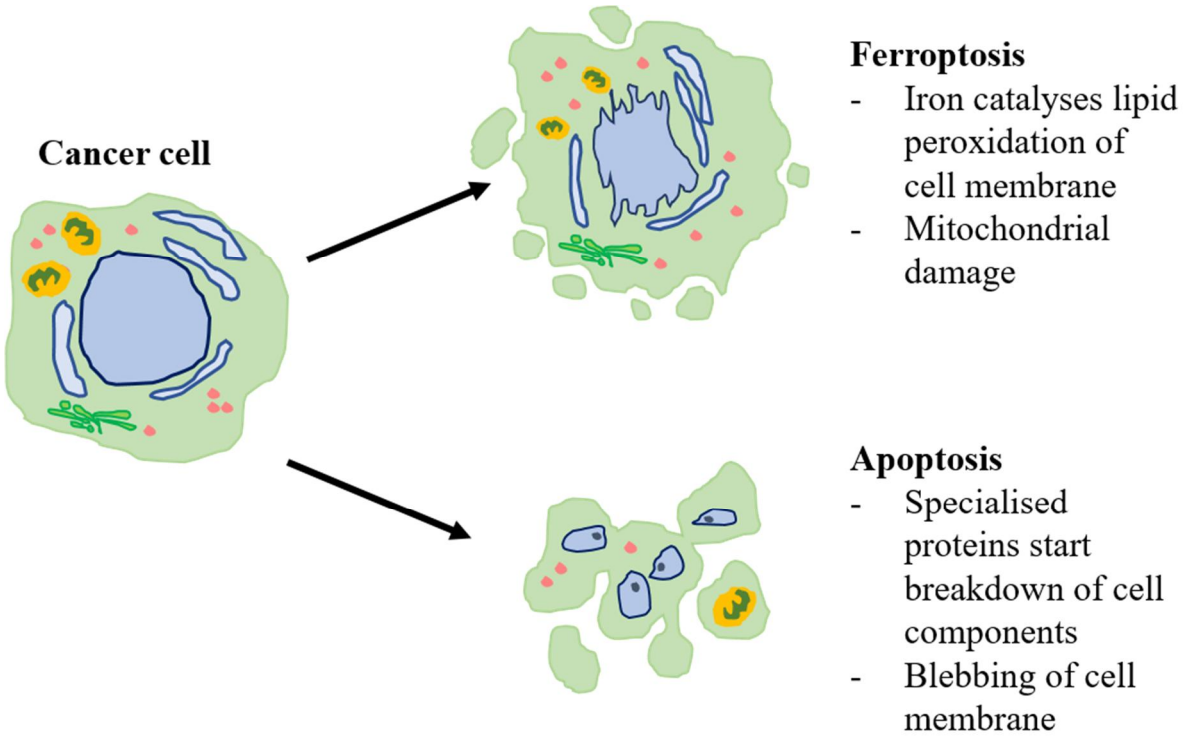

Figure 5. Differences between apoptosis and ferroptosis in cancer cell

Ferroptosis is different from programmed cell death (such as the aforementioned apoptosis) in a variety of ways. From the outside, apoptosing cells appear to dissolve, whereas ferroptotic cells experience cell death more internally in the cell (mainly in the mitochondria) and there is a less obvious external phenotype of cancer cell death. This figure was modified from *OncoBites*. April 22, 2020.

Reference

1. Brent R Stockwell, José Pedro Friedmann Angeli, Hülya Bayir, Ashley I Bush, Marcus Conrad et al. Ferroptosis: A Regulated Cell Death Nexus Linking Metabolism, Redox Biology, and Disease. *Cell*. 2017 Oct 5; 171(2):273-285.

2. Dixon SJ, Lemberg KM, Lamprecht MR, Skouta R, Zaitsev EM, Gleason CE, Patel DN, Bauer AJ, Cantley AM, Yang WS, Morrison B 3rd, Stockwell BR. Ferroptosis: an iron-dependent form of nonapoptotic cell death. *Cell*. 2012 May 25; 149(5):1060-1072.

3. Borong Zhou, Jiao Liu, Rui Kang, Daniel J. Ferroptosis is a type of autophagy-dependent cell death. *Seminars in Cancer Biology*. 2020 Nov; 66:89-100.

4. Haitao Yu, Pengyi Guo, Xiaozai Xie, Yi Wang, and Gang chen. Ferroptosis, a new form of cell death, and its relationships with tumourous diseases. *J Cell Mol Med*. 2017 Apr; 21(4): 648–657.

5. Susan Elmore. Apoptosis: A Review of Programmed Cell Death. *Toxicol Pathol*. 2007; 35(4): 495–516.

6. Y Xie , W Hou , X Song , Y Yu , J Huang , X Sun , R Kang , D Tang. Ferroptosis: process and function. *Cell Death Differ*. 2016 Mar; 23(3):369-379.

7. Antti Saraste, Kari Pulkki. Morphologic and biochemical hallmarks of apoptosis. *Cardiovascular Research*. 2000 Feb; 45(3):528-537.

8. Jan Lewerenz, Gamze Ates, Axel Methner, Marcus Conrad, and Pamela Maher. Oxytosis/Ferroptosis—(Re-) Emerging Roles for Oxidative Stress-Dependent Non-apoptotic Cell Death in Diseases of the Central Nervous System. *Front Neurosci*. 2018; 12: 214.

9. Nazanin Abbaspour, Richard Hurrell, and Roya Kelishadi. Review on iron and its importance for human health. *J Res Med Sci*. 2014 Feb; 19(2): 164–174.

10. Suzy V. Torti and Frank M. Torti. Iron and cancer: more ore to be mined. *Nat Rev Cancer*. 2013 May; 13(5): 342–355.

11. 1.Yehuda S, Mostofsky DI. Iron Deficiency and Overload: From Basic Biology to Clinical Medicine. 2010; New York, NY. Humana Press.

12. Mark D. Kleven, Shall Jue, and Caroline A. Enns. The Transferrin Receptors, TfR1 and TfR2 Bind Transferrin through Differing Mechanisms. *Biochemistry*. 2018 Mar 6; 57(9): 1552–1559.

13. Motoki Fujimaki, Norihiko Furuya, Shinji Saiki, Taku Amo, Yoko Imamichi, and Nobutaka Hattori. Iron Supply via NCOA4-Mediated Ferritin Degradation Maintains Mitochondrial Functions. *Mol Cell Biol*. 2019 Jul 15; 39(14): e00010-19.

14. Shu-Wing Ng, Sam G. Norwitz, and Errol R. Norwitz. The Impact of Iron Overload and Ferroptosis on Reproductive Disorders in Humans: Implications for Preeclampsia. *Int J Mol Sci*. 2019 Jul; 20(13): 3283.

15. Anna Martina Battaglia, Roberta Chirillo, Ilenia Aversa, Alessandro Sacco, Francesco Costanzo, and Flavia Biamonte. Ferroptosis and Cancer: Mitochondria Meet the "Iron Maiden" Cell Death. *Cells*. 2020 Jun; 9(6): 1505.

16. Cristina Espinosa-Diez, Verónica Miguel, Daniela Mennerich, Thomas Kietzmann, Patricia Sánchez-Pérez, Susana Cadenas, and Santiago Lamas. Antioxidant responses and cellular adjustments to oxidative stress. *Redox Biol*. 2015 Dec; 6: 183–197.

17. Michael Schieber and Navdeep S. Chandel. ROS Function in Redox Signaling and Oxidative Stress. *Curr Biol*. 2014 May 19; 24(10): 453–462.

18. Lian-Jiu Su, Jia-Hao Zhang, Hernando Gomez, Raghavan Murugan, Xing Hong, Dongxue Xu,

Fan Jiang, and Zhi-Yong Peng. Reactive Oxygen Species-Induced Lipid Peroxidation in Apoptosis, Autophagy, and Ferroptosis. *Oxid Med Cell Longev*. 2019; 2019: 5080843.

19. Marcus Conrad, Valerian E. Kagan, Hülya Bayir, Gabriela C. Pagnussat, Brian Head, Maret G. Traber, and Brent R. Stockwell. Regulation of lipid peroxidation and ferroptosis in diverse species. *Genes Dev*. 2018 May 1; 32(9-10): 602–619.

20. Wan Seok Yang, Katherine J. Kim, Michael M. Gaschler, Milesh Patel, Mikhail S. Shchepinov, and Brent R. Stockwell. Peroxidation of polyunsaturated fatty acids by lipoxygenases drives ferroptosis. *Proc Natl Acad Sci U S A*. 2016 Aug 23; 113(34): 4966–4975.

21. Liyuan Wang, Yichen Liu, Tingting Du, Heng Yang, Lei Lei, Mengqi Guo, Han-Fei Ding, Junran Zhang, Hongbo Wang, Xiaoguang Chen, Chunhong Yan. ATF3 promotes erastin-induced ferroptosis by suppressing system Xc^-. *Cell Death Differ*. 2020 Feb; 27(2): 662–675.

22. Tao Xu, Wei Ding, Xiaoyu Ji, Xiang Ao, Ying Liu, Wanpeng Yu, and Jianxun Wang. Molecular mechanisms of ferroptosis and its role in cancer therapy. *J Cell Mol Med*. 2019 Aug; 23(8): 4900–4912.

23. Wan Seok Yang, Rohitha SriRamaratnam, Matthew E. Welsch, Kenichi Shimada, Rachid Skouta et al. Regulation of Ferroptotic Cancer Cell Death by GPX4. *Cell*. 2014 Jan 16; 156(0): 317–331.

Part 1.

The role of autophagy

in erastin-induced ferroptosis

Abbreviations

ATG	Autophagy-related protein
ER	Endoplasmic reticulum
PE	phosphatidylethanolamine
mTOR	mammalian target of rapamycin
ROS	reactive oxygen species
NCOA4	Nuclear receptor coactivator 4
FTH1	ferritin heavy chain 1
IRP2	iron responsive element binding protein 2
Tf	transferrin
TfR1	transferrin receptor 1
IREs	iron responsive elements
HSPB1	heat shock protein B1
HDFn	human dermal neonatal fibroblastic cells
3-MA	3-methylaldehyde
PI3K	phosphatidylinositol 3-kinase
CQ	chloroquine
Baf A1	bafilomycin A1
NAC	N-acetyl-l-cysteine
DFP	deferiprone
DFO	deforoxamine

Abstract

Ferroptosis is a novel form of programmed cell death in which the accumulation of intracellular iron promotes lipid peroxidation, leading to cell death. Recently, the induction of autophagy has been suggested during ferroptosis. However, this relationship between autophagy and ferroptosis is still controversial and the autophagy-inducing mediator remains unknown. In this study, Furthermore, autophagy leads to iron-dependent ferroptosis by degradation of ferritin and induction of transferrin receptor 1 (TfR1) expression, in wild-type and autophagy-deficient cells, BECN1+/− and LC3B−/−. Consistently, autophagy deficiency caused depletion of intracellular iron and reduced lipid peroxidation, resulting in cell survival during erastin-induced ferroptosis. Moreover, autophagy was triggered by erastin-induced reactive oxygen species (ROS) in ferroptosis. These data provide evidence that ROS-induced autophagy is a key regulator of ferritin degradation and TfR1 expression during ferroptosis. These results contributes that toward our understanding of the ferroptotic processes and also helps resolve some of the controversies associated with this phenomenon.

Introduction

1. Autophagy

Autophagy is the natural, regulated mechanism of the cell that removes unnecessary or dysfunctional components. Autophagy, "self-eating" at the subcellular level, has gained tremendous attention in the past few years, and our knowledge concerning the mechanism of autophagy has expanded dramatically [1]. Autophagy is an evolutionarily conserved degradation pathway that maintains homeostasis [2]. Autophagy plays a complex role in human health and disease. Autophagy promotes cell survival in response to environmental stressors. While, in some cases, excessive and impaired autophagy may contribute to cell death [3]. Autophagy is mediated by a unique organelle called the autophagosome. As autophagosomes engulf a portion of cytoplasm, autophagy is generally thought to be a nonselective degradation system [4] (Figure 1). At the molecular level, autophagy is executed by autophagy-related (ATG) proteins that can undergo multiple posttranslational modifications [5]. Autophagy can either act nonspecifically to remove cytoplasmic structures or selectively degrade substrates such as aggregated proteins, damaged organelles, and invading pathogens [6]. Recently, accumulating evidence indicates that autophagy contributes to ferroptosis [7].

1.1 Molecular mechanism of autophagy

Autophagy is the major regulated-cellular pathway for degrading long-lived proteins and is the only known pathway for degrading cytoplasmic organelles [8]. Autophagy consists of several sequential steps, which are induction, autophagosome formation, autophagosome and lysosome fusion and degradation [4]. Autophagy is induced under a number of stresses, including starvation, organelle/DNA damage, hypoxia, ER stress, and pathogen infection [9]. In mammalian cells, phagophore membranes appear to initiate primarily from the ER. The formation of the double-membrane vesicle is a complex process involving 16 autophagy-related proteins (Atg proteins). Apart from this, two ubiquitin-like

conjugation systems are involved in autophagy. These systems produce modified complexes of autophagy regulators: Atg8-PE and Atg5-Atg12-Atg16, and that may determine the formation and size of the autophagosome [6]. There are two ubiquitin-like systems that are key to autophagy acting at the Atg5–Atg12 conjugation step and at the LC3 processing step [4]. Conjugated Atg5–Atg12 complexes in pairs with Atg16L dimers to form a multimeric Atg5–Atg12–Atg16L complex that associates with the extending phagophore. The association of Atg5–Atg12–Atg16L complexes is thought to induce curvature into the growing phagophore through asymmetric recruitment of processed LC3B-II [10]. Atg5–Atg12 conjugation is not dependent on activation of autophagy and once the autophagosome is formed, Atg5–Atg12–Atg16L dissociates from the membrane, making conjugated Atg5–Atg12 a relatively poor marker of autophagy [6]. The second ubiquitin-like system involved in autophagosome formation is the processing of microtubule-associated protein light chain 3 (LC3B) [6, 10].

LC3B is expressed in most cell types as a full-length cytosolic protein that, upon induction of autophagy, is proteolytically cleaved by Atg4, a cysteine protease, to generate LC3B-I. Activated LC3B-I is then transferred to Atg3, a different E2-like carrier protein before phosphatidylethanolamine (PE) is conjugated to the carboxyl glycine to generate processed LC3B-II [6]. Recruitment and integration of LC3B-II into the growing phagophore is dependent on Atg5–Atg12 and LC3B-II is found on both the internal and external surfaces of the autophagosome, where it plays a role in both hemifusion of membranes and in selecting cargo for degradation [10]. The synthesis and processing of LC3 is increased during autophagy, making it a key readout of levels of autophagy in cells. It is proposed that LC3B-II, acting as a ‘receptor’ at the phagophore, interacts with ‘adaptor’ molecules on the target to promote their selective uptake and degradation [11]. The most characteristic molecule in this regard is p62/SQSTM1, a multi-functional adaptor molecule that promotes turnover of poly-ubiquitinated protein aggregates [12] (Figure 2).

When the autophagosome completes fusion of the expanding ends of the phagophore membrane, the next step towards maturation in this self-degradative process is fusion of the autophagosome with the

specialized endosomal compartment that is the lysosome to form the 'autolysosome' [4]. Within the lysosome, cathepsin proteases B and D are required for turnover of autophagosomes and, by inference, for the maturation of the autolysosome. Lamp-1 and Lamp-2 at the lysosome are also critical for functional autophagy, as evidenced by the inhibitory effect of targeted deletion of these proteins in mice on autolysosome maturation [13].

2. Autophagy and cancer

Autophagy plays important roles in the degradation of damaged organelles and old proteins and in the maintenance of cellular homeostasis [6]. In cancer biology, autophagy plays dual roles in tumor promotion and suppression and contributes to the development and proliferation of cancer cells [14] (Figure 3). Some anticancer drugs can regulate autophagy [15]. Therefore, autophagy-regulated chemotherapy can be involved in cancer-cell survival or death. Tumor suppressor factors are negatively regulated by mTOR and AMPK, resulting in the induction of autophagy and suppression of the cancer initiation [16]. In contrast, oncogenes may be activated by mTOR, class I PI3K, and AKT, resulting in the suppression of autophagy and enhancement of cancer formation [17]. Reduced and abnormal autophagy inhibits degradation of damaged components or proteins in oxidative-stressed cells, leading to the development of cancer.

2.1 Autophagy as a regulator of tumor suppression

The basal level of autophagy operates as a mechanism for tumor suppression via reduction of damaged cellular parts and proteins and maintenance of cellular homeostasis [18]. Previous studies have reported that the depletion of the autophagy-related gene Beclin1 is observed in a variety of cancers. Beclin1 is important in the formation of the phagophore, suggesting that Beclin1 functions as a tumor suppressor [19]. In cancer-cell lines and mice models, the loss of Beclin1 results in a reduction of autophagy and an increase in cell proliferation, further indicating that Beclin1 gene acts as a tumor suppressor [20]. Other studies have shown that the deficiency of autophagic regulators, such as ATG3, ATG5, ATG9, is associated with oncogenesis [21]. In addition, autophagy prevents tumor formation through the

regulation of reactive oxygen species (ROS). Mitochondrial damage promotes excessive ROS production, resulting in promotion of carcinogenesis. Autophagy is a crucial mechanism that inhibits tumorigenesis, and impaired autophagy may result in oncogenesis [22, 23].

2.2 Autophagy as a regulators of tumor promotion

Several studies have shown that autophagy plays a role in promote tumor survival and growth in advanced cancers [24, 25]. Tumors are exposed to extremely stressful conditions, including hypoxia and nutrient deprivation. Autophagy helps cells to overcome these stresses [14]. Autophagy is also increased in RAS-mutated cancer cells that maintain a high basal-level of autophagy. RAS are small GTPases involved in important signal pathways for proliferation, survival, and metabolism [26]. Some studies have revealed that a high level of autophagy is observed in RAS-activating mutated cells, and cell survival is dependent on autophagy during nutrient starvation. Autophagy plays an important role in cell survival of several tumors that depend on RAS activation [27, 28].

3. Autophagy in ferroptosis

A recent study revealed that autophagy was helps with ferroptosis by degrading ferritin in cancer cells [29] (Figure 4 and 5). Knockdown of autophagy-related (ATG) 5 and ATG7 limited erastin-stimulated ferroptosis by reducing the intracellular ferrous iron concentration and lipid peroxidation [30]. Autophagy plays an important role in the regulation of ferroptosis by regulating cellular iron homeostasis and cellular ROS generation [31]. Upon induction of ferroptosis, autophagy is activated, leading to degradation of cellular iron stock protein ferritin and thus an increase of cellular labile iron level via NCOA4-mediated autophagy pathway, ferritinophagy [32]. High levels of cellular labile iron ensure rapid accumulation of cellular ROS, which is essential for ferroptosis [32]. Upon cystine deprivation, autophagy is activated to degrade the iron storage protein ferritin, which is mediated by the cargo receptor NCOA4. Such NCOA4-mediated autophagic degradation of ferritin. By maintaining cellular labile iron contents, promotes the accumulation of cellular ROS and consequent ferroptotic cell death. Ferroptosis is a form of autophagic cell death, as ferroptosis satisfies the two major criteria of

autophagic cell death that the death process is associated with autophagy activation and that autophagy plays a pro-death role in the cell death process [32]. While autophagy activation appears to be modest as measured by LC3 conjugation, it is highly likely that the cargo-specific autophagy, ferritinophagy, is preferentially activated [32]. Increase in endogenous ferritin heavy chain 1 (FTH1) expression during ferroptosis [33]. Subsequently, overexpression of FTH1 enhanced ferritin degradation after induction of ferroptosis by erastin [30]. It has been found that autophagy driven ferroptosis occurs during the early initiation stage [34].

3.1 The regulatory mechanism of ferritinophagy

NCOA4 mediated ferritinophagy for degrading ferritin is a responsive mechanism to dynamic iron states [35] (Figure 6). When ferritinophagy is impaired via NCOA4 depletion, iron availability is reduced, whereas iron responsive element binding protein 2 (IRP2) activity is induced to promote the translation of transferrin (Tf) [36]. IRP2, a protein of the iron regulatory network, is controlled by cellular iron levels by binding to iron responsive elements (IREs) [37]. The regulation of IRE IRP2 in transferrin (Tf) is also closely linked to the initiation of ferroptosis. On lower iron concentration, the recycling of Tf is significantly inhibited by heat shock protein B1 (HSPB1), which represents an inhibitory mechanism of ferroptosis [38]. In response to the high iron level, E3 ubiquitin ligase 2 (HERC2) mediates NCOA4 turnover in ubiquitin dependent manners through CUL7 homology domain in HERC2 and a C terminal domain in NCOA4, thereby preventing ferritinophagy and blocking excess iron liberating ferritin [35].

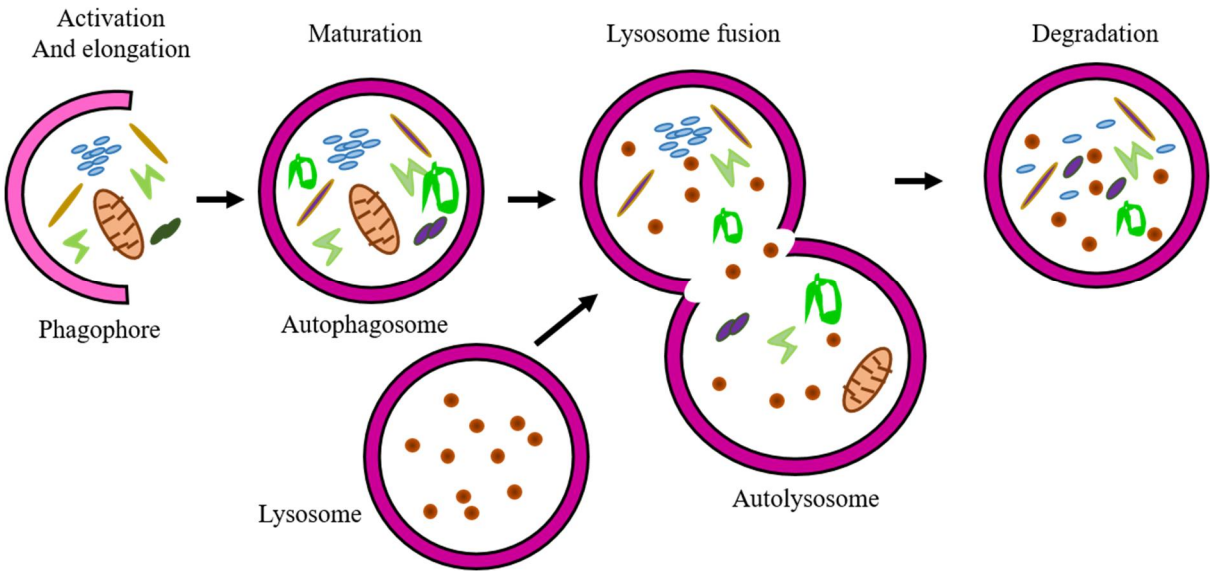

Figure 1. Steps of the autophagic flux.

Autophagy is activated in response to various cellular stress conditions. A double-membrane vesicle (phagophore) begins to form and elongate into an autophagosome in order to engulf intracellular degradation components, including mitochondria, damaged organelles and lipid droplets. The mature autophagosome with intracellular degradation components then fuses with the lysosome and forms an autolysosome, which provides an acidic environment for hydrolytic enzymes to hydrolyze the engulfed components. This figure was modified from *Oncol Rep*. 2019 Nov;42(5):1647-1655.

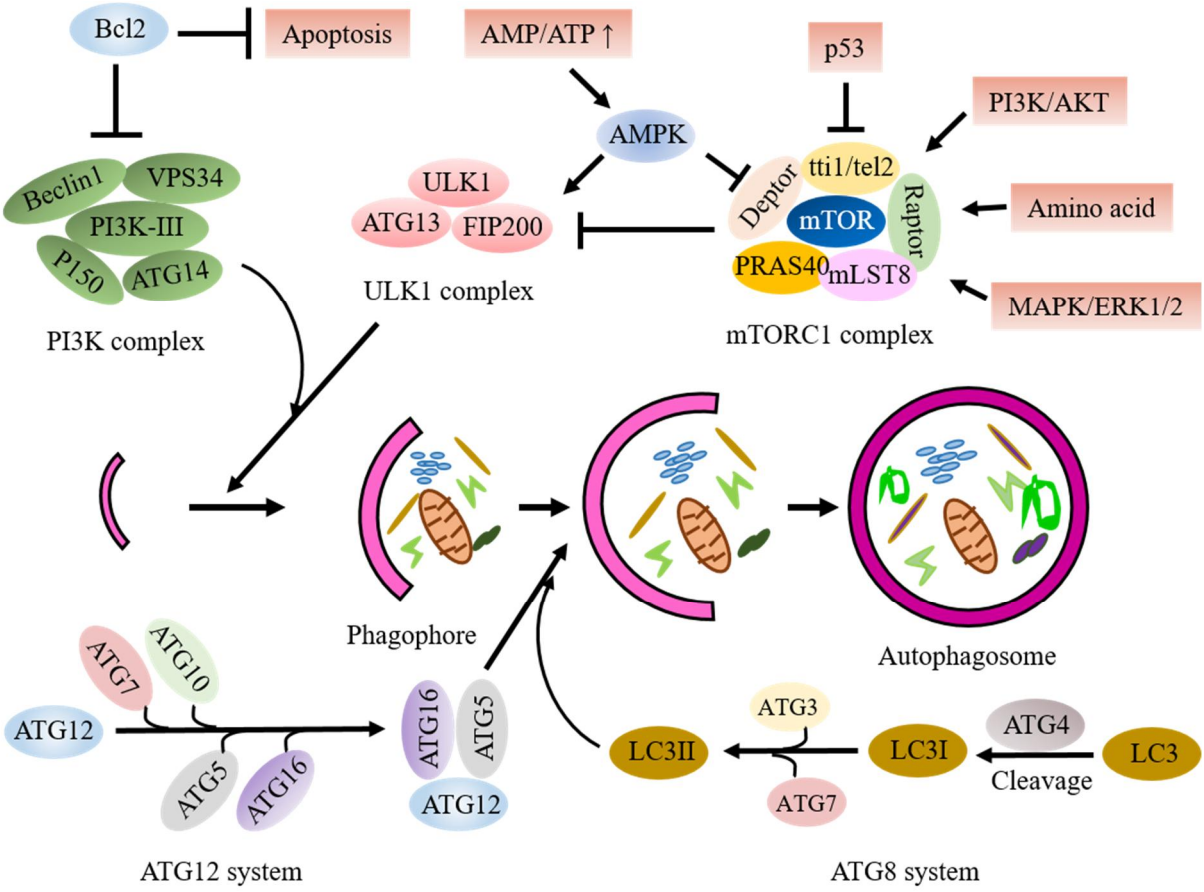

Figure 2. Signaling pathways of autophagy.

mTOR kinase is a pivotal molecule in the mTORC1 complex that plays an important role in the regulation of autophagy. Autophagy activation is triggered by decreased activity of the mTORC1 complex due to the activation of AMPK or p53 signaling. The decreased activity of mTORC1, an inhibitor of the mammalian ULK1 complex, leads to the increase the activity of the ULK1 complex, which subsequently initiates the formation of phagophore in conjunction with the PI3K complex. The elongation and maturation of the phagophore is dependent on two ubiquitin-like conjugation systems (ATG12 and ATG8), which involve multiple autophagy proteins, including ATG5, ATG16 and LC3. This figure was modified from *Oncol Rep*. 2019 Nov;42(5):1647-1655.

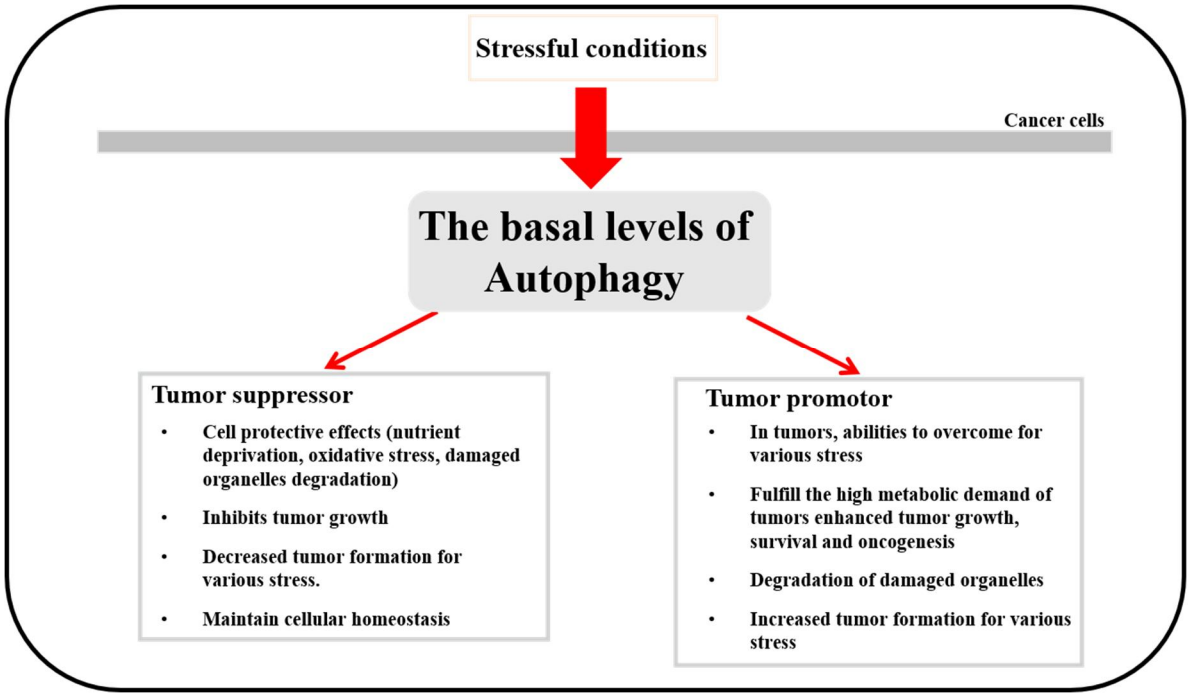

Figure 3. Autophagy roles of tumor promotor and suppressor in cancer cells

In cancer biology, autophagy plays dual roles in tumor promotion and suppression and contributes to cancer-cell development and proliferation. Some anticancer drugs can regulate autophagy. Therefore, autophagy-regulated chemotherapy can be involved in cancer-cell survival or death. Additionally, the regulation of autophagy contributes to the expression of tumor suppressor proteins or oncogenes. This figure was modified from Int J Mol Sci. 2018 Nov 5;19(11):3466.

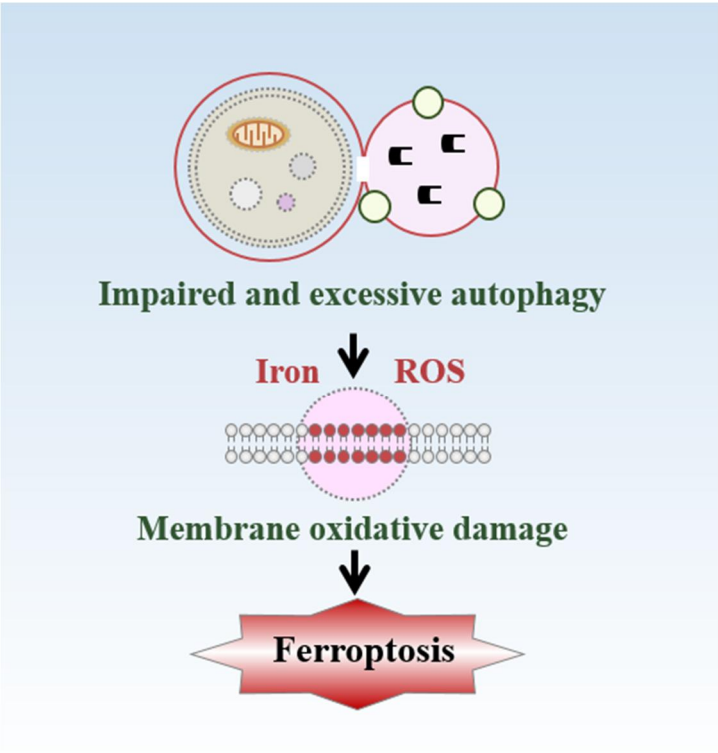

Figure 4. Regulatory mechanisms and signaling pathways of autophagy-dependent ferroptosis

The recently discovered role of autophagy, especially selective types of autophagy (e.g., ferritinophagy, lipophagy, clockophagy, and chaperone-mediated autophagy), in driving cells toward ferroptotic death motivated us to explore the functional interactions between metabolism, immunity, and cell death. This figure was modified from Cell Chem Biol. 2020 Apr 16;27(4):420-435.

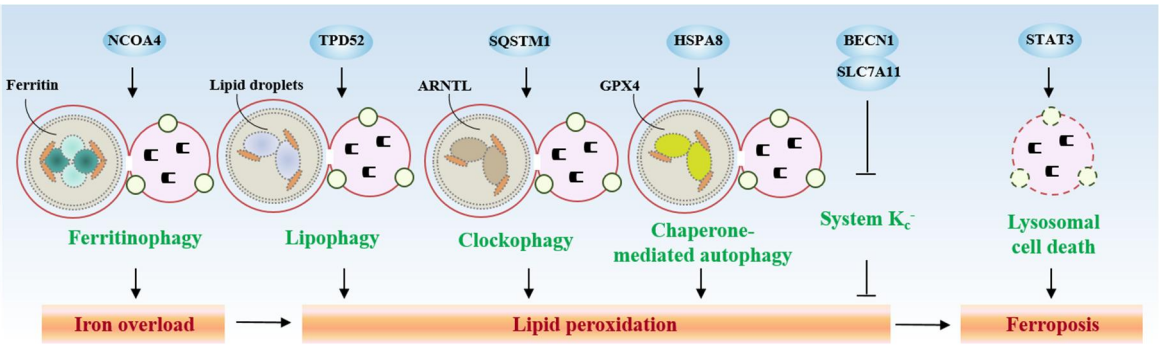

Figure 5. Role of autophagy and lysosome in the regulation of ferroptosis.

Certain types of selective autophagy, such as ferritinophagy, lipophagy, clockophagy, and chaperone-mediated autophagy, contribute to iron accumulation and lipid peroxidation during ferroptosis. In addition, the autophagy core regulator BECN1 can promote ferroptosis through the inhibition of system Xc^-. Moreover, STAT3-mediated lysosomal cell death contributes to ferroptosis through the release of the hydrolytic enzymes into the cytosol. This figure was modified from *Ferroptosis in Health and Disease*. 2019 Oct. 43-59.

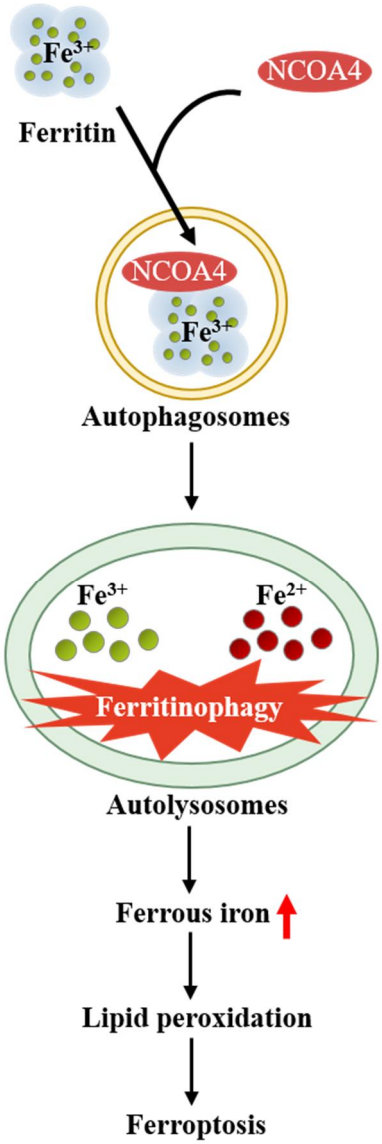

Figure 6. Ferritinophagy, the NCOA4-dependent degradation of ferritin, accumulates ferrous iron to induce ferroptosis.

Ferritinophagy is the process of autophagic degradation of the iron storage protein ferritin, which is critical for the regulation of cellular iron levels. NCOA4-dependent ferritinophagy promotes ferroptosis through releasing free iron from ferritin. The depletion or inhibition of NCOA4 or ATG protein inhibits ferritin degradation and therefore reduces free iron levels and thus limits subsequent oxidative injury during ferroptosis. This figure was modified from *Oxid Med Cell Longev*. 2020 Aug 17; 2020: 9738143.

Results

Autophagy-dependent ferroptosis was induced by erastin.

Autophagy is the natural, regulated, destructive biological process that disassembles unnecessary or dysfunctional components of a cell [39]. Autophagy is generally a stress-responsive survival mechanism [40]. However, a controversial theory is that autophagy may also be a cell death mechanism i.e., autophagic cell death. To identify the role of autophagy in erastin-induced ferroptosis, protein expression levels of LC3B, a stable marker protein associated with the biochemical detection of cellular autophagy were examined in HT1080 cells in response to ferroptosis. Total protein were isolated from HT1080 cells with erastin for the different times. Western blot revealed that erastin treatment increased the levels of LC3B expression in HT1080 cells (Figure 1A). HT1080 cells were transfected with LC3B shRNA or control shRNA to investigate the effects of LC3B expression under erastin-treated condition. To check down regulation of LC3B expression in LC3B shRNA transfected HT1080 cells, compared with control shRNA transfected HT1080 cells. Total protein were harvested and LC3B levels were analyzed LC3B shRNA or control shRNA transfected HT1080 cells. Protein levels of LC3B were decreased in LC3B shRNA transfected HT1080 cells compared with control shRNA transfected HT1080 cells (Figure 1B). To further investigate the critical role of LC3B, the PI positive cells were analyzed in response to erastin in LC3B shRNA transfected HT1080 cells compared with control shRNA transfected HT1080 cells. The PI positive cells of LC3B shRNA transfected HT1080 cells was decreased in presence of erastin, compared with that of control shRNA transfected HT1080 cells treated with erastin (Figure 1C). To confirm whether autophagy correlated with cell death during the erastin treatment, treated cells with erastin in the presence or absence of rapamycin, autophagy activator, or chloroquine (CQ), autophagy inhibitor confirmed PI positive cells. Treatment with rapamycin further increased the PI positive cells, compared erastin treatment alone in HT1080 cells (Figure 1D). In

contrast, Treatment with CQ not change the PI positive cells (Figure 1E). These results showed that autophagy involved in erastin-induced cell death.

Erastin-induced ferroptotic cell death was decreased in autophagy-deficient cells.

To understand ferroptosis signaling pathway involved to autophagy, primary fibroblast cells were isolated in autophagy-deficient mice, BECN1+/–, LC3B–/–, and wild type mice. And then, to examine that whether autophagy was deficient in these cells, autophagy-deficient cells were treated with rapamycin, inducer of autophagy, as inhibition of mTOR for the various time points. Western blot revealed that rapamycin treatment increased the level of LC3B expression in WT fibroblast. However, the level of LC3B expression was insignificant in $BECN1^{+/-}$ fibroblast and no expression in $LC3B^{-/-}$ fibroblast (Figure 2A and 2B). Ferroptosis is a newly discovered iron-dependent process of cell death [41]. To investigate the role of autophagy in erastin-induced ferroptotic cell death, lung fibroblastic cells from $BECN1^{+/-}$, $LC3B^{-/-}$, and wild type mice were used. The $BECN1^{+/-}$, $LC3B^{-/-}$, and wild type fibroblasts were treated with different concentrations of vehicle or erastin for different time durations, and the cell viability was measured. The viability of $BECN1^{+/-}$ and $LC3B^{-/-}$ fibroblastic cells was enhanced in presence of 2μM erastin and 10μM erastin, compared with that of wild type cells treated with 2μM or 10μM erastin (Figure 3A). Further, the cell viability decreased after 5μM erastin treatment for 8h and 24h in wild-type cells, but not in $BECN1^{+/-}$ and $LC3B^{-/-}$ fibroblastic cells (Figure 3B). To examine whether erastin could induce the cell death in other primary human dermal neonatal fibroblastic cells (HDFn) or foreskin adult fibroblastic cells (NuFF), these cells were treated with erastin and then performed a cell viability assay. Significant increases in cell death were observed in both human primary fibroblastic cells by WST-1 assay (Figure 3C). No significant differences in cell death were observed between human and mouse cells. In addition, to ascertain whether the enhanced cell viability in $BECN1^{+/-}$ and $LC3B^{-/-}$cells is specific to erastin treatment, these and wild type cells were treated with the cell death inducer, auranofin. A similar level of cell death was observed in $BECN1^{+/-}$, $LC3B^{-/-}$, and wild type fibroblastic cells 24h after auranofin administration (Figure 3D), suggesting that

the effects were erastin-specific. These data together suggest that the erastin-induced cell death in primary fibroblastic cells is associated with the autophagy process.

Inhibition of autophagy disrupts erastin-triggered cell death.

To verify whether erastin induces autophagy, whether autophagy levels were examined change in the presence of erastin in wild type, BECN1$^{+/-}$, or LC3B$^{-/-}$ fibroblastic cells. These fibroblastic cells were treated with vehicle or various doses of erastin (2, 5, or 10μM) and harvested total protein 24 h after cell treatment. LC3B is a central protein in the autophagy pathway and is widely used as a biomarker of autophagosome [42]. In wild type fibroblastic cells, the levels of LC3B-II (lower band of LC3B) protein was found to increase upon treatment with low dose of erastin (2μM), and a more striking increase was evident at higher doses of erastin (5μM and 10μM), compared with treatment with vehicle (Figure 4A and 4B). However, enhanced levels of LC3B-II were not observed in BECN1$^{+/-}$ and LC3B$^{-/-}$ fibroblastic cells after erastin treatment (Figure 4A and 4B), suggesting that the erastin-induced LC3B-II expression is dependent on the autophagy process. To confirm whether increases in LC3B activation correlated with increased autophagic flux during the erastin treatment, these experiments were repeated by treating cells with erastin in the presence or absence of 3-methylaldehyde (3-MA), an inhibitor of phosphatidylinositol 3-kinase (PI3K) that blocks autophagosome formation, or chloroquine (CQ), an inhibitor of autophagosome-lysosome fusion. Treatment with 3-MA further decreased the activation of LC3B-II in vehicle or erastin-treated wild type fibroblasts, indicative of autophagic activity (Figure 4C). Consistently, CQ treatment further elevated the activation of LC3B-II in wild type fibroblasts (Figure 4C). In contrast, the erastin-treated BECN1$^{+/-}$ and LC3B$^{-/-}$ fibroblastic cells did not show decreased or elevated activation of LC3B-II upon 3-MA or CQ treatments, respectively (Figure 4C and 4D). Next, to determine the role of autophagy in erastin-triggered cell death, Cell viability was determined by the WST-1 assay whether the autophagy inhibitors affected erastin-induced cell death in wild type, BECN1$^{+/-}$, and LC3B$^{-/-}$ fibroblasts. As shown in Figure 4E, in wild type fibroblasts, the erastin-induced cell death recovered in the presence of autophagy inhibitors, 3-MA or CQ, compared with erastin treatment alone. However, similar treatment had no effect on BECN1$^{+/-}$, and LC3B$^{-/-}$ fibroblast cells (Figure 4E). These data indicate that erastin-induced ferroptosis is an autophagy-dependent process and

autophagy is a key activator of erastin-induced cell death.

Depletion of autophagy attenuates lipid peroxidation in erastin-induced ferroptosis.

ROS accumulation is one of the hallmarks of ferroptosis. Consistently, ferroptosis inhibitors (such as ferrostatin-1) and various antioxidants or ROS scavengers can all completely inhibit cellular ROS accumulation and ferroptotic cell death [43]. Thus, it was hypothesized that depletion of autophagy protein levels such as BECN1 or LC3B may contribute to the regulation of erastin-induced ROS production and cell death in fibroblastic cells. To investigate the role of autophagy in lipid peroxidation, wild type, $BECN1^{+/-}$, and $LC3B^{-/-}$ fibroblastic cells were treated with vehicle or erastin and the cytosolic reactive oxygen species (ROS) (Figure 5A) and lipid peroxidation (Figure 5B) were assayed by flow cytometry using the fluorescent probes CellROX and C11-BODIPY, respectively. As shown in Figure 5A and 5B, erastin treatment increased cytosolic ROS and lipid peroxidation compared with vehicle in wild type fibroblastic cells, but not in $BECN1^{+/-}$and $LC3B^{-/-}$ fibroblastic cells. To verify whether the erastin-induced lipid peroxidation is dependent on the autophagy pathway, wild type fibroblastic cells were treated with autophagy inhibitors, CQ, or bafilomycin A1 (Baf A1), blocker of the fusion between autophagosomes and lysosomes, in the absence or presence of erastin. The erastin-induced cytosolic ROS and lipid peroxidation were disrupted upon inhibition of the autophagy process by the administration of CQ and Baf A1, compare with erastin treatment alone (Figure 5C and 5D).

Autophagy deficiency inhibits erastin-induced intracellular levels of iron.

Erastin-induced ferroptotic cell death involves the accumulation of intracellular iron, resulting in the production of cytosolic and lipid ROS [41]. Therefore, the intracellular iron content was examined in wild-type and autophagy-deficient cells upon various treatments. Intracellular levels of total iron were increased 24 h after erastin (5μM) administration in wild-type fibroblastic cells, but not in BECN1+/− and LC3B−/− fibroblastic cells. Furthermore, erastin-induced intracellular iron in wildtype fibroblastic cells was found to decrease in the presence of the antioxidant, NAC (Figure 6A). However, NAC treatment of BECN1+/− and LC3B−/− fibroblastic cells had no effect on the intracellular iron content (Figure 6A). The intracellular levels of iron can increase upon degradation of iron protein complexes, such as ferritin, which forms a complex of 24 subunits consisting of a mixture of ferritin heavy (FTH) and light chains (FTL) [44]. Especially, ferritin is degraded via a recently identified autophagic process, ferritinophagy, and FTH1 is a substrate of ferritinophagy leading to lysosomal degradation [45, 46]. Therefore, I determined whether low levels of intracellular iron in autophagy-deficient cells were related to autophagy-mediated degradation of FTH1 in the presence of erastin. Wild-type or autophagy-deficient LC3B−/− fibroblastic cells were treated with vehicle or erastin and harvested total protein 2, 4, 6, 8, or 10 h after treatment. The protein levels of FTH1 were found to decrease over time in wild-type fibroblastic cells in the presence of erastin (Figure 6B). However, protein levels of FTH1 were enhanced in autophagy deficient, LC3B−/−, fibroblastic cells (Figure 6B). To confirm that the degradation of ferritin occurred via the autophagy pathway, the cells were pretreated with the autophagy inhibitor 3-MA for 1 h before erastin treatment, and then the protein levels of FTH1 were determined. After erastin administration, protein levels of FTH1 decreased in wild-type fibroblastic cells, but increased in 3-MA-pretreated wild-type fibroblastic cells (Figure 6C). The transferrin receptor (TfR1) is needed for the import of iron into the cell and is regulated in response to intracellular iron concentration [47]. Therefore, the protein levels of TfR1 were analyzed in autophagy deficient cells (LC3B−/−) and autophagy inhibited cells (by inhibitor 3-MA), after erastin administration (Figure 6B and 6C). The protein levels of TfR1 were increased after 6 h of erastin administration in wild-type

fibroblastic cells (Figure 6B and 6C). However, decreased levels of TfR1 were found 2 h after erastin administration in autophagy inhibitor (3MA)-treated wild-type fibroblastic cells (Figure 6C). Interestingly, the protein levels of TfR1 were not increased in autophagy-deficient cells (LC3B−/−) after erastin administration (Figure 6C). To verify whether autophagy is involved in iron-dependent cell death by erastin, we next observed the cell viability 24 h after erastin treatment in the absence or presence of iron chelator, deferiprone (DFP). Erastin-induced cell death recovered in the presence of iron chelator, DFP, in wildtype fibroblastic cells, but not in autophagy-deficient fibroblastic cells and DFP recovery was more partial than ROS inhibition and other previous treatments (Figure 6D). These data suggest that autophagy is a key regulator for controlling the intracellular iron levels through ferritin degradation and the expression of TfR1 in response to erastin.

ROS-dependent ferroptosis was blocked in autophagy-deficient cells.

To further confirm whether autophagy-induced ROS production is involved in erastin-induced cell death, the impact of the antioxidant N-acetylcysteine (NAC) or the mitochondria-specific antioxidant mito-TEMPO was examined on erastin-induced cell death in wild type, $BECN1^{+/-}$, and $LC3B^{-/-}$ fibroblastic cells. Pre-treatment with NAC or mito-TEMPO significantly recovered cell viability in wild type fibroblastic cells (Figure 7A and 7B). However, pre-treatment with NAC or mito-TEMPO had no significant effects on erastin-induced cell death in $BECN1^{+/-}$ and $LC3B^{-/-}$ fibroblastic cells (Figure 7A and 7B). These data suggest that autophagy might positively regulate erastin-triggered cell death by increasing lipid peroxidation.

Erastin-enhanced ROS leads to autophagy.

To further investigate whether erastin-induced ROS triggered autophagy, wild type fibroblastic cells were treated with vehicle, erastin (5μM) or erastin plus ROS inhibitors (NAC and mito-TEMPO), iron chelator (deforoxamine, DFO), or inhibitor for lipid peroxidation (ferrostatin-1) and harvested total protein 2, 4, 6, 8, or 10 h after cell treatment. Erastin treatment increased the levels of LC3B-II (lower band of LC3B) protein, while treatment with ROS inhibitors (NAC and mito-TEMPO) blocked autophagy in wild type fibroblastic cells (Figure 8A and 8B). However, erastin-induced autophagy was not blocked in the presence of iron chelator (deforoxamine, DFO) or inhibitor for lipid peroxidation (ferrostatin-1) (Figure 8C and 8D). These data suggest that erastin-induced ROS triggers autophagy and results in increasing intracellular iron.

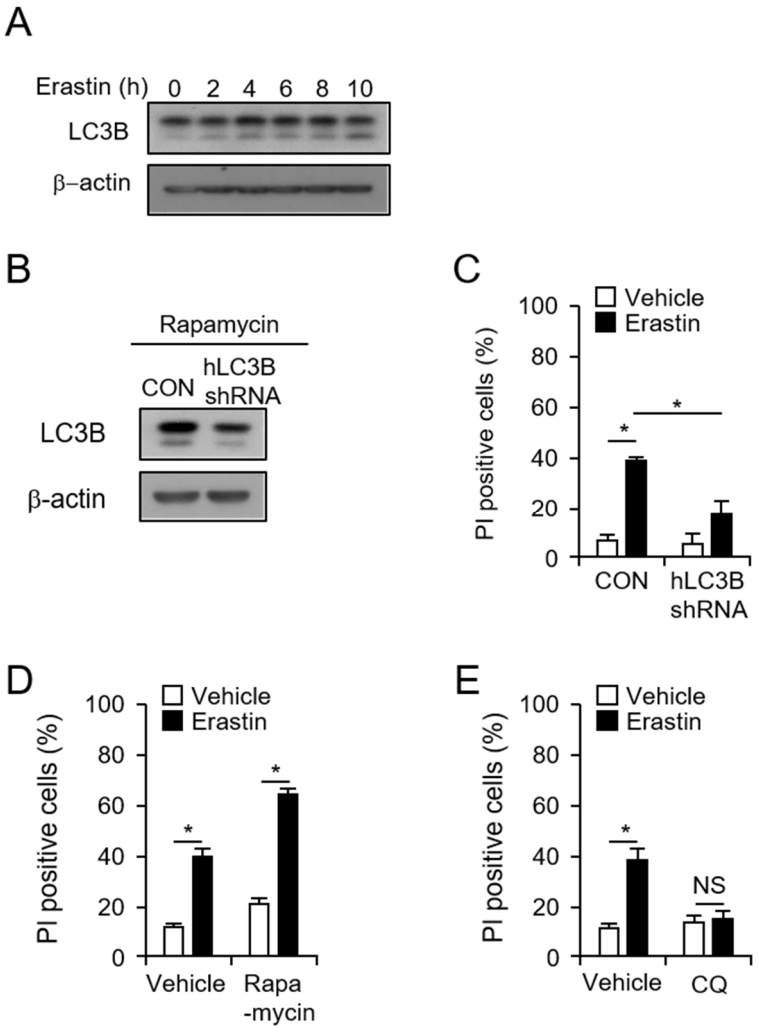

Figure 1. Erastin-induced ferroptosis was accelerated in the presence of rapamycin-induced autophagy.

HT1080 cells were treated erastin (10μM) for the indicated length of time points. LC3B was assessed by western blot analysis. β-actin was used as a loading control (A). HT1080 cells were transfected with control or LC3B shRNA. Protein levels of LC3B was analyzed to verify the downregulation of LC3B expression (B). The PI positive cells were analyzed in response to erastin (10μM) in HT1080 control or LC3B shRNA transfected cells (C). HT1080 cells were treated with erastin in the presence of rapamycin (C) or CQ (D) and stained with propidium iodide (PI) to confirm cell death. PI stained cells were analyzed using a flow cytometer. Values are mean ± SD, n=8. *P < 0.05 indicates significant increase compared with vehicle or erastin alone.

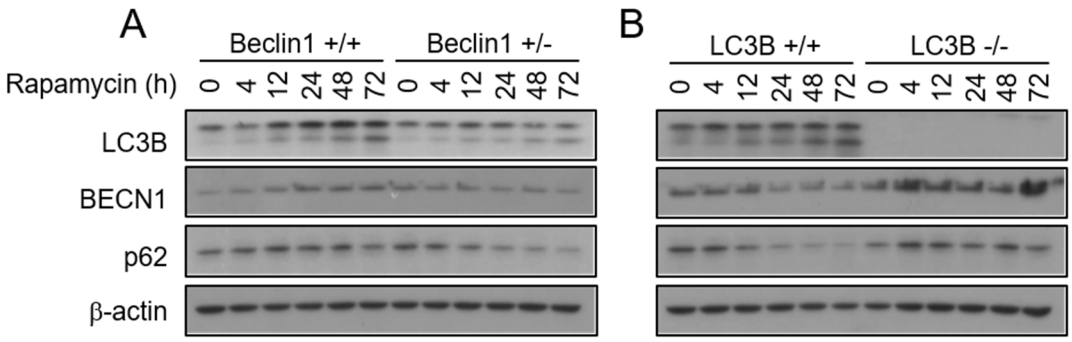

Figure 2. Rapamycin-induced autophagy was impaired in BECN+/– and LC3–/– fibroblastic cells. Vehicle or rapamycin was treated in BECN+/+, BECN+/–, LC3B+/+, and LC3B–/– fibroblastic cells at various time points. LC3B, BECN1, and p62 were assessed by Western blot analysis. β-actin was used as controls for normalization.

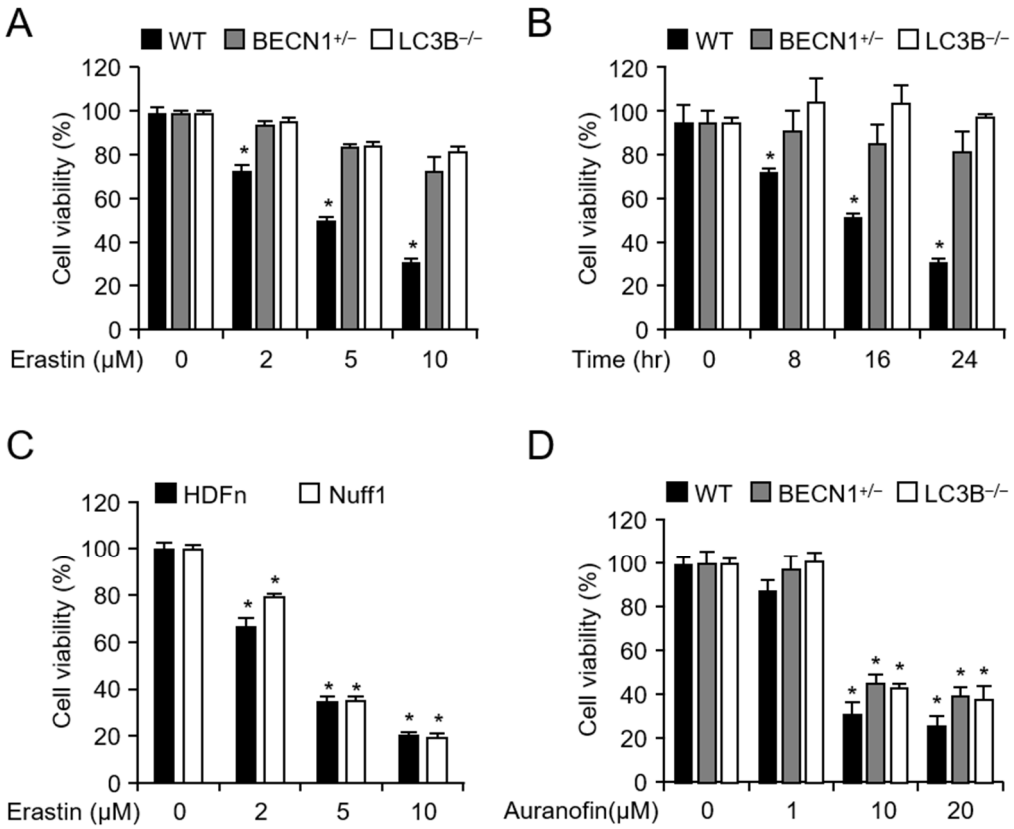

Fig. 3 Erastin-induced ferroptotic cell death was decreased in autophagy-deficient cells.

Cell viability assay was performed using wild type(n= 12), BECN1+/− (n = 12), and LC3B−/− (n = 12), primary mouse fibroblastic cells treated with indicated doses of erastin for 24 h (A) or treated for different time durations with 5μM erastin (B). Cell viability was investigated in primary human dermal neonatal fibroblast (HDFn) and foreskin adult fibroblast (NuFF) following treatment with erastin (24 h) at the indicated concentration (C). Cell viability was investigated in wild type (n = 12), BECN1+/− (n = 12), and LC3B−/− (n = 12), primary mouse fibroblastic cells following treatment with indicated doses of auranofin for 24 h (D). All data shown are the mean ± SD from three independent experiments. *P < 0.05 indicates significant decrease compared with vehicle.

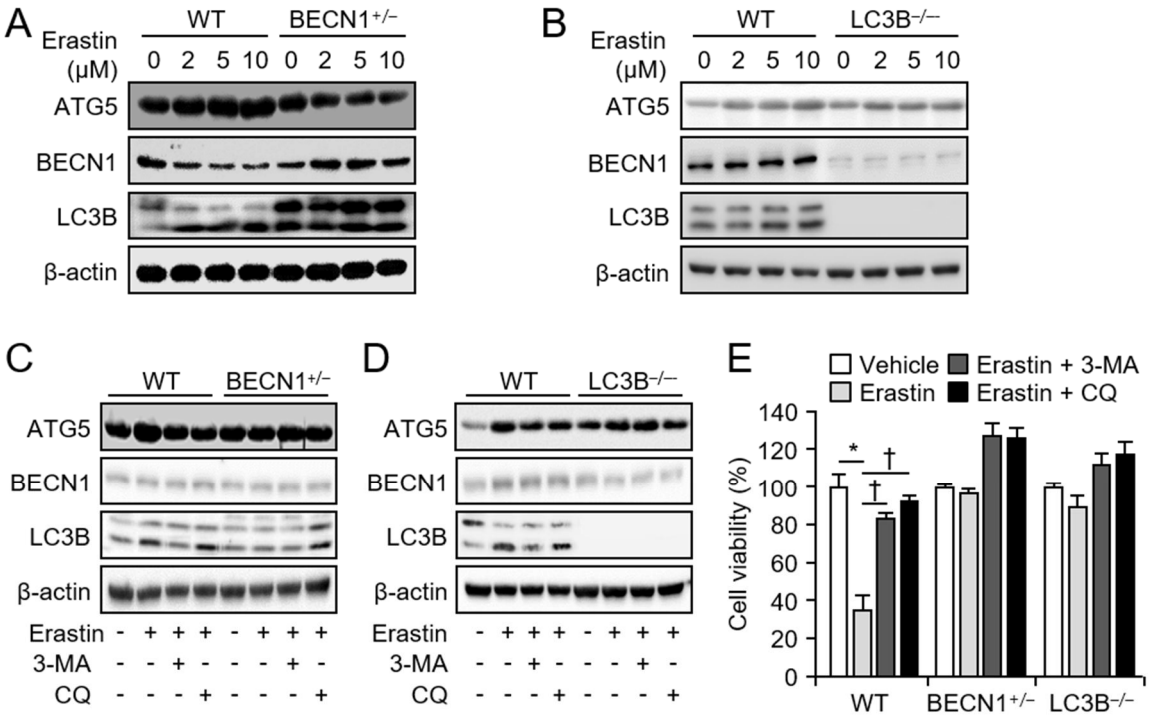

Fig. 4 Inhibition of autophagy decreased erastin-induced ferroptotic cell death.

Wild type or autophagy-deficient cells (BECN1+/– or LC3B−/−) were treated with various doses of erastin for 24 h and autophagy-related proteins, ATG5, BECN1, and LC3B, were analyzed by western blot (A, B). Wild type or autophagy-deficient cells (BECN1+/− (n = 3) or LC3B−/− (n =3)) were pretreated with autophagy inhibitors (3-MA or CQ) 1 h before erastin (5μM) treatment for 24 h, and autophagy-related proteins, ATG5, BECN1, and LC3B, were analyzed by western blot (C, D). Cell viability was assayed 24 h after vehicle, erastin, or erastin plus autophagy inhibitor (3-MA or CQ) treatment in wild type (n = 12), BECN1+/− (n =12), or LC3B−/− (n = 12) (E). All data shown are the mean ± SD from three independent experiments. *$P < 0.05$ indicates significant decrease compared with vehicle; †$P < 0.05$ indicates significant increase compared with erastin treatment.

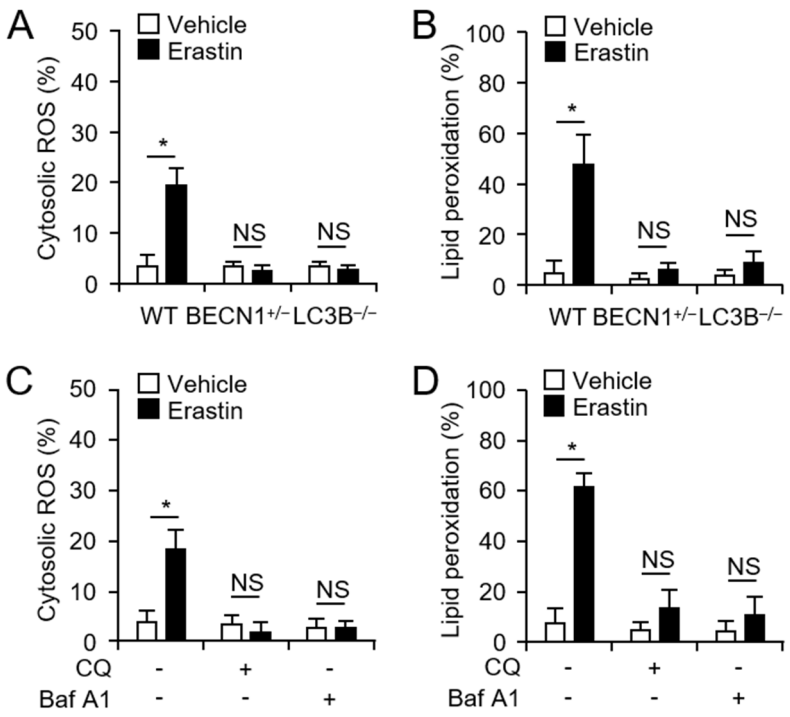

Fig. 5 Erastin-induced lipid peroxidation was disrupted in autophagy-deficient cells.

Wild type, BECN1+/−, or LC3B−/− fibroblastic cells were treated with vehicle or erastin (5μM) for 24 h. Cytosolic ROS (A) and lipid peroxidation (B) were assayed for by flow cytometry using the fluorescent probes CellROX® Deep Red (cytosolic ROS) and C11-BODIPY (lipid peroxidation), respectively. Wild-type fibroblastic cells were treated with vehicle, erastin (5μM), or erastin plus autophagy inhibitor (CQ or Baf A1) for 24 h and cytosolic ROS and lipid peroxidation were measured (C, D). Fluorescence of each probe was measured using FlowJo software program. The mean percentages ± SD of positive cells per total cells are shown in plots. Values are mean ± SD, n =6. *P < 0.05 indicates significant increase compared with vehicle; NS, not significant.

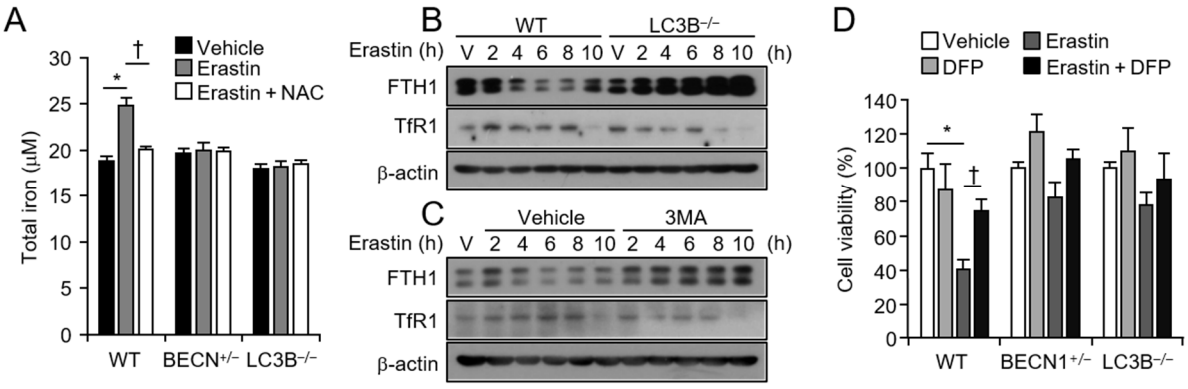

Figure 6. Levels of erastin-enhanced intracellular iron were restrained in autophagy deficient cells.

Levels of erastin-enhanced intracellular iron were restrained in autophagy-deficient cells. The wild type, BECN1+/−, or LC3B−/− fibroblastic cells were treated with vehicle or erastin (5μM) in the absence or presence of the ROS scavenger, NAC, for 24 h and intracellular iron levels were assessed using a commercial assay (A). *P < 0.05 indicates significant increase compared with vehicle. †P < 0.05 indicates significant decrease compared with erastin alone. The wild type, LC3B+/+, and LC3B−/− fibroblastic cells were treated with vehicle or erastin (5μM) for indicated time. Total protein was harvested and the protein levels of FTH1 and TfR1 were analyzed using western blot; β-actin was used as an internal loading control (B). The wild type fibroblastic cells were treated with vehicle or erastin (5μM) in the absence or presence of autophagy inhibitor, 3-MA (10μM). Total protein was harvested and the protein levels of FTH1 and TfR1 were analyzed using western blot; β-actin was used as an internal loading control (C). These experiments were performed as three individual experiments and representative data is shown here. The wild type, BECN1+/−, or LC3B−/− fibroblastic cells were treated with vehicle, DFP (5μM), or erastin (5μM) in the absence or presence of DFP for 24 h and cell viability was assessed (D). All data shown are the mean ± SD. *P < 0.05 indicates significant decrease compared with vehicle; †P < 0.05 indicates significant increase compared with erastin alone.

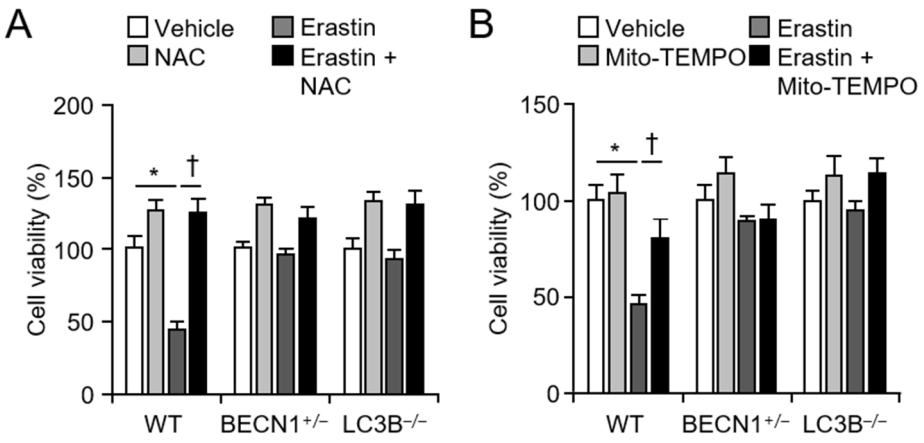

Figure 7. ROS-dependent ferroptosis was blocked in autophagy-deficient cells.

The wild type, BECN1+/–, and LC3B–/– fibroblastic cells were treated with vehicle, NAC (1mM), Mito-TEMPO (10μM), erastin (5μM), or erastin plus NAC or mito-TEMPO (A, B). Cell viability was analyzed 24 h after treatment. All experiments were performed at least three independent times. All data shown are the mean ± SD, n = 9. *P < 0.05 indicates significant decrease compared with vehicle; † P < 0.05 indicates significant increase compared with erastin-treated cells.

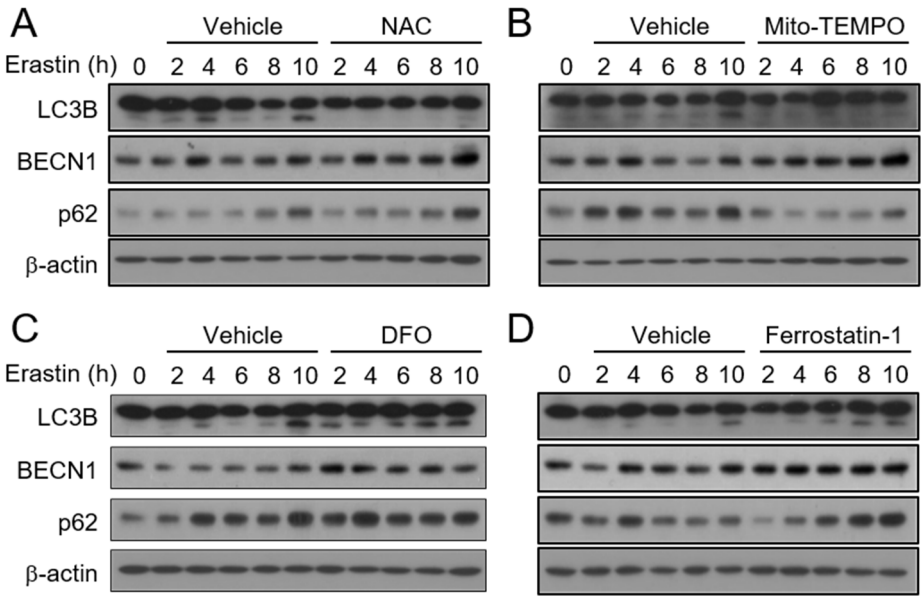

Figure 8. Autophagy was activated by erastin-mediated ROS in ferroptosis.

The wild type fibroblastic cells were treated with vehicle or erastin (5 μM) in the absence or presence of ROS scavenger, NAC (A) or mito-TEMPO (B), iron chelator, DFO (C), or ferroptosis inhibitor, ferrostatin-1 (D). Total protein was harvested and the protein levels of LC3B, BECN1, and p62 were analyzed using western blot; β-actin was used as an internal loading control. These experiments were performed as three individual experiments and representative data is shown here.

Discussion

Ferroptosis is characterized as a type of programmed cell death that results from iron-dependent lipid peroxidation and is different from other types of cell death, especially autophagy [48]. In this study, a ferroptotic inducer, erastin, enhances the amount of LC3B-II in wild type fibroblastic cells. Furthermore, viability of autophagy-deficient LC3B$^{-/-}$ fibroblastic cells increased in the presence of erastin, compared with that of wild type cells. Autophagy is a cellular catabolic degradation response to starvation or stress whereby cellular proteins, organelles and cytoplasm are engulfed, digested and recycled to sustain cellular metabolism [49]. Autophagy pathway is also used for the elimination of pathogens and for the engulfment of apoptotic cells [50, 51]. However, the effect of these events on ferroptosis is not well understood. Although recent publications report a role of autophagy in ferroptotic cell death in breast cancer cells and wild type mouse embryonic fibroblasts, their observations were contradictory [30, 32]. Among the initial publications, Jiang's group demonstrated that erastin-enhanced LC3 conversion in mouse embryonic fibroblasts (MEFs) and HT1080 cells and erastin-induced cell death were inhibited in the presence of autophagy inhibitors, suggesting that ferroptosis is an autophagic cell death process [32]. On the other hand, Gibson's group insisted that the autophagy-induced cell death during ferroptosis occurred independently in breast cancer cells [52]. In their study, siramesine, a lysosome disruptor, and lapatinib, a dual tyrosine kinase inhibitor, initially induced ferroptotic cell death, but switched to autophagic cell death later on in breast cancer cells. Different inducers and cell types may induce different cellular mechanisms for ferroptotic cell death. However, in present study, erastin-induced ferroptotic cell death was clearly inhibited in autophagy-deficient BECN$^{+/-}$ and LC3B$^{-/-}$ fibroblastic cells (Figure 3). This phenomena was confirmed by inhibition of erastin-induced ferroptotic cell death in the presence of autophagy inhibitors in wild type, BECN$^{+/-}$, or LC3B$^{-/-}$ fibroblastic cells (Figure 4E). This data strongly support the initial theory that ferroptosis is as an autophagic cell death

process. Furthermore, erastin-increased reactive oxygen species (ROS) induces LC3B conversion and activated autophagy (Figure 8). With respect to the role of autophagy in ferroptosis, they demonstrated that autophagy regulates ferroptosis by regulating cellular iron homeostasis and cellular ROS generation [32]. Iron is a requisite metal in almost all biological systems. However, the levels of iron in the cell need to be tightly regulated, as an excess of iron can have damaging effects due to the generation of ROS [53]. Especially, autophagy can lead to the degradation of cellular iron stock protein ferritin and thus cause an increase of cellular labile iron levels, via NCOA4-mediated autophagy pathway, termed as ferritinophagy. High levels of cellular labile iron ensure rapid accumulation of cellular ROS, which is essential for ferroptosis [32]. This study showed that the levels of intracellular iron were less in the autophagy-deficient cells compared with wild type fibroblastic cells (Figure 6A). Consistently, the heavy subunit of ferritin, ferritin heavy chain 1 (FTH1), was degraded by erastin in wild type cells, but not in autophagy-deficient cells, or in wild type cells in presence of the autophagy inhibitor, 3MA (Figure 6B and 6C), indicating that autophagy regulates the intracellular iron levels during erastin-induced ferroptotic process. Transferrin receptor is a carrier protein for transferrin, an iron-binding plasma protein, thus controlling the level of intracellular iron levels [47]. Interestingly, the protein levels of transferrin receptor (TfR1) were enhanced by erastin in wild type cells, but not in autophagy deficient cells and autophagy inhibitor-treated wild type cells (Figure 6C). Thus, our results demonstrate that autophagy regulates intracellular iron levels through ferritin degradation and transferrin receptor induction. Although autophagy has been reported during ferroptosis, the mediator of autophagy induction was not known. Gibson's group suggested that prolonged iron-mediated ROS generation can induce autophagy [52]. However, present data showed that ROS inhibitors, NAC and mito-TEMPO, decreased erastin-induced autophagy, although the iron chelator, DFO, or lipid peroxidation inhibitor, ferrostatin-1 could not (Figure 8). This indicates that iron-independent ROS is involved in induction of erastin-mediated autophagy.

Reference

1. Zhifen Yang and Daniel J. Klionsky. An Overview of the Molecular Mechanism of Autophagy. *Curr Top Microbiol Immunol*. 2009; 335: 1–32.

2. Yoomi Chun and Joungmok Kim. Autophagy: An Essential Degradation Program for Cellular Homeostasis and Life. *Cells*. 2018 Dec; 7(12): 278.

3. Gautam Das, Bhupendra V. Shravage, and Eric H. Baehrecke. Regulation and Function of Autophagy during Cell Survival and Cell Death. *Cold Spring Harb Perspect Biol*. 2012 Jun; 4(6): a008813.

4. Noboru Mizushima. Autophagy: process and function. *Genes & Dev*. 2007. 21: 2861-2873

5. Hana Popelka and Daniel J. Klionsky. Posttranslationally-modified structures in the autophagy machinery: an integrative perspective. *FEBS J*. 2015 Sep; 282(18): 3474–3488.

6. Danielle Glick, Sandra Barth, and Kay F. Macleod. Autophagy: cellular and molecular mechanisms. *J Pathol*. 2010 May; 221(1): 3–12.

7. Rui Kang and Daolin Tang. Autophagy and Ferroptosis - What's the Connection? *Curr Pathobiol Rep*. 2017 Jun; 5(2): 153–159.

8. Jong-Ok Pyo, Jihoon Nah and Yong-Keun Jung. Molecules and their functions in autophagy. *Experimental & Molecular Medicine* 2012 44, 73–80.

9. Jason S. King, Douwe M. Veltman, and Robert H. Insall. The induction of autophagy by mechanical stress. *Autophagy*. 2011 Dec 1; 7(12): 1490–1499.

10. Barth S, Glick D, Macleod KF. *Autophagy: assays and artifacts*. J Pathol. 2010 DOI: 10.1002/path.2694.

11. Kirkin V, McEwan DG, Novak I, Dikic I. A role for ubiquitin in selective autophagy. *Mol Cell*. 2009;34:259–269

12. Ralston SH. Pathogenesis of Paget's disease on bone. *Bone*. 2008;43: 819–825.

13. Tanaka Y, Guhde G, Suter A, Eskelinen EL, Hartmann D, Lullmann-Rauch R, et al. Accumulation of autophagic vacuoles and cardiomyopathy in LAMP-2-deficient mice. *Nature*. 2000;406: 902–906.

14. Chul Won Yun and Sang Hun Lee. The Roles of Autophagy in Cancer. *Int J Mol Sci*. 2018 Nov; 19(11): 3466.

15. Rosenfeldt M.T., Ryan K.M. The multiple roles of autophagy in cancer. *Carcinogenesis*. 2011;32:955–963

16. Yenniffer Ávalos, Jimena Canales, Roberto Bravo-Sagua, Alfredo Criollo, Sergio Lavandero, and Andrew F. G. Quest. Tumor Suppression and Promotion by Autophagy. *Biomed Res Int*. 2014 Sep; 2014: 603980.

17. Choi A.M., Ryter S.W., Levine B. Autophagy in human health and disease. N. *Engl. J. Med*. 2013;368: 651–662.

18. Tang D., Kang R., Livesey K.M., Cheh C.W., Farkas A., Loughran P., Hoppe G., Bianchi M.E., Tracey K.J., Zeh H.J., 3rd, et al. Endogenous HMGB1 regulates autophagy. *J. Cell Biol*. 2010;190: 881–892.

19. Shen Y., Li D.D., Wang L.L., Deng R., Zhu X.F. Decreased expression of autophagy-related proteins in malignant epithelial ovarian cancer. *Autophagy*. 2008;4:1067–1068

20. Liang X.H., Jackson S., Seaman M., Brown K., Kempkes B., Hibshoosh H., Levine B. Induction of autophagy and inhibition of tumorigenesis by beclin 1. *Nature*. 1999;402:672–676

21. Kuma A., Hatano M., Matsui M., Yamamoto A., Nakaya H., Yoshimori T., Ohsumi Y., Tokuhisa T., Mizushima N. The role of autophagy during the early neonatal starvation period. *Nature*. 2004; 432:1032–1036.

22. Moloney J.N., Cotter T.G. ROS signalling in the biology of cancer. *Semin. Cell Dev. Biol*. 2018; 80: 50–64.

23. Filomeni G., De Zio D., Cecconi F. Oxidative stress and autophagy: The clash between damage and metabolic needs. *Cell Death Differ*. 2015; 22: 377–388.

24. Luo T., Fu J., Xu A., Su B., Ren Y., Li N., Zhu J., Zhao X., Dai R., Cao J., et al. PSMD10/gankyrin induces autophagy to promote tumor progression through cytoplasmic interaction with ATG7 and nuclear transactivation of ATG7 expression. *Autophagy*. 2016; 12: 1355–1371.

25. Liu M., Jiang L., Fu X., Wang W., Ma J., Tian T., Nan K., Liang X. Cytoplasmic liver kinase B1 promotes the growth of human lung adenocarcinoma by enhancing autophagy. *Cancer Sci*. 2018; 109: 3055–3067.

26. Su C.C. Tanshinone IIA can inhibit MiaPaCa2 human pancreatic cancer cells by dual blockade of the Ras/Raf/MEK/ERK and PI3K/AKT/mTOR pathways. *Oncol. Rep*. 2018; 40: 3102–3111.

27. Goncalves P.R., Rocha-Brito K.J., Fernandes M.R., Abrantes J.L., Duran N., Ferreira-Halder C.V. Violacein induces death of RAS-mutated metastatic melanoma by impairing autophagy process. *Tumour Biol*. 2016;37: 14049–14058

28. Shin J.H., Park C.W., Yoon G., Hong S.M., Choi K.Y. NNMT depletion contributes to liver cancer cell survival by enhancing autophagy under nutrient starvation. *Oncogenesis*. 2018; 7:58.

29. Yan Song, Hu Yang, Rui Lin, Kui Jiang and Bang Mao Wang. The role of ferroptosis in

digestive system cancer. *ONCOLOGY LETTERS* 2019. 18: 2159-2164.

30. Wen Hou, Yangchun Xie, Xinxin Song, Xiaofang Sun, Michael T. Lotze, Herbert J. Zeh, III, Rui Kang, and Daolin Tang. Autophagy promotes ferroptosis by degradation of ferritin. *Autophagy*. 2016 Aug; 12(8): 1425–1428.

31. Yulu Zhou, Yong Shen, Cong Chen, Xinbing Sui, Jingjing Yang, Linbo Wang, and Jichun Zhou. The crosstalk between autophagy and ferroptosis: what can we learn to target drug resistance in cancer? *Cancer Biol Med*. 2019 Nov; 16(4): 630–646.

32. Minghui Gao, Prashant Monian, Qiuhui Pan, Wei Zhang, Jenny Xiang, and Xuejun Jiang. Ferroptosis is an autophagic cell death process. *Cell Res*. 2016 Sep; 26(9): 1021–1032.

33. Jie Li, Feng Cao, He-liang Yin, Zi-jian Huang, Zhi-tao Lin, Ning Mao, Bei Sun and Gang Wang. Ferroptosis: past, present and future. *Cell Death Dis*. 2020 Feb; 11(2): 88.

34. Daolin Tang, Rui Kang. Regulation and Function of Autophagy During Ferroptosis. *Ferroptosis in Health and Disease.* 2019 Oct. 43-59

35. Maria Quiles del Rey and Joseph D. Mancias. NCOA4-Mediated Ferritinophagy: A Potential Link to Neurodegeneration. *Front Neurosci*. 2019 Mar 14;13: 238.

36. Naiara Santana-Codina and Joseph D. Mancias. The Role of NCOA4-Mediated Ferritinophagy in Health and Disease. *Pharmaceuticals*. 2018 Dec; 11(4): 114.

37. Gaetano Cairo and Stefania Recalcati. Iron-regulatory proteins: molecular biology and pathophysiological implications. *Expert Rev Mol Med*. 2007 Dec; 9(33): 1–13.

38. Xiaofang Sun, Zhanhui Ou, Min Xie, Rui Kang, Yong Fan, Xiaohua Niu, Haichao Wang, Lizhi Cao, and Daolin Tang. HSPB1 as a Novel Regulator of Ferroptotic Cancer Cell Death. *Oncogene*. 2015 Nov 5; 34(45): 5617–5625.

39. *Klionsky, DJ. Autophagy revisited: A conversation with Christian de Duve. Autophagy. 2008;*

4, 740–743

40. Ellen Wirawan, Tom Vanden Berghe, Saskia Lippens, Patrizia Agostinis, Peter Vandenabeele. Autophagy: for better or for worse. *Cell Res*. 2012 Jan; 22(1):43-61.

41. Dixon SJ. et al. Ferroptosis: an iron-dependent form of nonapoptotic cell death. *Cell* 2012; 149, 1060-1072

42. Klionsky DJ. et al. Guidelines for the use and interpretation of assays for monitoring autophagy. *Autophagy*. 2016; 12, 1-222

43. Kwon MY, Park E, Lee SJ, Chung SW. Heme oxygenase-1 accelerates erastin-induced ferroptotic cell death. *Oncotarget*. 2015**; 6,** 24393-24403

44. Ganz T. Nemeth E. Hepcidin and iron homeostasis. *Biochim Biophys Acta*. 2012; 1823, 1434–1443.

45. Mancias, J.D., Wang, X., Gygi, S.P., Harper, J.W., Kimmelman, A.C. Quantitative proteomics identifies NCOA4 as the cargo receptor mediating ferritinophagy. *Nature.* 2014; 509, 105–109.

46. Mancias JD. et al. Ferritinophagy via NCOA4 is required for erythropoiesis and is regulated by iron dependent HERC2-mediated proteolysis. *Elife*. 2015; 4, e10308.

47. Qian ZM, Li H, Sun H, Ho K. Targeted drug delivery via the transferrin receptor-mediated endocytosis pathway. *Pharmacological Reviews*. 2002; 54, 561-587.

48. Yang WS, Stockwell BR. Ferroptosis: Death by Lipid Peroxidation. *Trends Cell Biol*. 2016; 26, 165-176.

49. Levine B, Klionsky DJ. Development by self-digestion: molecular mechanisms and biological functions of autophagy. *Dev Cell*. 2004; 6, 463–477.

50. Colombo MI. Autophagy: a pathogen driven process. *IUBMB Life*. 2007; 59, 238–242.

51. Qu X. et al. Autophagy gene-dependent clearance of apoptotic cells during embryonic development. *Cell*. 2007; 128, 931–946.

52. Ma S. Ferroptosis and autophagy induced cell death occur independently after siramesine and lapatinib treatment in breast cancer cells. *PLoS One*. 2017; 12, e0182921

53. Reed JC, Pellecchia M. Ironing out cell death mechanisms. *Cell*. 2012; 149, 963-965.

Part 2.

The role of PGC1α

in erastin-induced ferroptosis

Abbreviations

PGC-1	PPARγ coactivator-1
BAT	Brown adipose tissue
ERR	Estrogen related receptor
RCC	Renal cell carcinoma
MMP	Mitochondrial membrane potential
mPTP	Mitochondrial permeability transition pore
TH	Thyroid hormone
SIRTs	sirtuines
CDKs	cyclin-dependent kinases
AMPK	adenosine-monophosphate-activated kinase
NRFs	nuclear respiratory factors
CaMKs	calcium-calmodulin-activated kinases
Mfrn	Mitoferrin
FtMt	Mitochondrial ferritin
LDH	Lactate dehydrogenase
mPTP	Mitochondrial permeability transition pore
HO-1	Heme oxygenase-1
CORM	CO releasing molecules

Abstract

Ferroptosis is a novel form of regulated cell death, characterized by an iron-dependent increase in lipid peroxidation. In the aspect of iron metabolism, mitochondria play a key role. Ferroptosis was characterized by condensed mitochondrial membrane densities and smaller volume than normal mitochondria. PGC1α is the master regulator of mitochondrial biogenesis. However, relationship between PGC1α and ferroptosis remains has not been studied yet. In this study, the role of PGC1α was investigated in ferroptosis. The expression of PGC1α was increased by the ferroptosis inducer, erastin. Furthermore, PGC1α inhibitor suppresses erastin-induced cell death. The most important biochemical features of ferroptosis are the elevated levels of lipid hydroperoxides (LOOH) and ferrous ion (Fe^{2+}) concentration. Thus, erastin-triggered lipid peroxidation and intracellular levels of ferrous ion were regulated by PGC1α inhibitor in HT1080 fibrosarcoma cells. And this phenomenon was the equal in PGC1α shRNA transfected HT1080 cells. Moreover, PGC1α was triggered by erastin-induced mitochondria dysfunction during ferroptosis. Erastin-induced mitochondria dysfunction such as loss of mitochondria membrane potential and mitochondrial ROS production, was blocked in PGC1α inhibition. Previously, HO-1 is known as an essential enzyme in the iron-dependent lipid peroxidation during ferroptosis. In the present study, HO-1 induced by ferroptosis is regulated by PGC1α. Taken together these results suggested that PGC1α is an essential for erastin-induced mitochondria dysfunction during ferroptotic cancer cell death.

Introduction

1. PGC1α

1.1 PPARγ coactivator-1 (PGC-1) family

Members of the PPARγ coactivator-1 (PGC-1) family of transcriptional coactivators act as inducible coregulators of nuclear receptors in the control of cellular energy metabolic pathways [1]. The transcriptional coactivator PGC1α was identified through its functional interaction with the nuclear receptor PPARγ in brown adipose tissue (BAT), a mitochondria-rich tissue specialized for thermogenesis [1, 2]. After that, 2 related coactivators, PGC1β (also termed PERC) and PGC1–related coactivator (PRC), were discovered. PGC1α and PGC1β are preferentially expressed in tissues with high oxidative capacity, such as heart, slow-twitch skeletal muscle, and BAT, where they play an important roles in the regulation of mitochondrial functional capacity and cellular energy metabolism. Less is known about the expression patterns and biologic roles of PRC [1, 3] (Figure 1).

1.2 Regulation mechanism of PGC1α

PGC1α activity is associated with a number of pathological conditions including diabetes and heart failure. PGC1α has been implicated in mitochondrial biogenesis and increased mitochondrial respiration [4]. PGC1α is a coactivator for many factors including, CBP, Scr-1, PPARα, glucocorticoid receptor, thyroid hormone receptor, several orphan receptors, and MEF2. PGC1α expression levels are regulated in response to a plethora of stimuli, exemplifying the spectrum of situations to which mitochondrial biogenesis and activity must respond [5]. The mechanisms governing the transcription of PGC1α have been extensively studied and vary between distinct tissues and different situations, even though there is a common pattern of regulation emerging [5]. PGC1α is controlled by several posttranslational modifications. Because PGC1α is markedly sensitive to cellular energy status, it is

tightly regulated by stress sensors such as AMP activated protein kinase (AMPK) and SIRT1. Both AMPK-mediated phosphorylation and SIRT1-mediated deacetylation activate PGC1α under energy deprivation conditions. In addition, the p38 MAPK stabilizes the PGC1α protein by increasing its phosphorylation state [7, 8]. These diverse posttranslational modifications direct PGC1α to different target genes [9]. And, some transcription factors coactivated by PGC1α can, in turn, regulate PGC1α, comprising autoregulatory loops that augment target gene transcription (Figure 2 and 3).

1.3 The function of PGC1α

The regulation of cellular and mitochondrial metabolism is controlled by numerous transcriptional networks [10]. The most well-known and studied member of the PGC1 family is PGC1α (encoded by the PPARGC1A gene). PGC1α is a positive regulator of mitochondrial biogenesis and respiration, adaptive thermogenesis, gluconeogenesis as well as many other metabolic processes [11]. Importantly, the expression of PGC1α is highly inducible by physiological cues, including exercise, cold and fasting [12]. A central function of PGC1α that is intimately linked to mitochondrial biogenesis is the detoxification of reactive oxygen species (ROS). Indeed, ROS are generated during mitochondrial respiration, and PGC1α has emerged as a key player, controlling their removal by regulating the expression of numerous ROS-detoxifying enzymes [13, 14, 15]. Therefore, it appears that PGC1α both increases mitochondrial functions and minimizes the buildup of its by-products, ensuring a global positive impact on oxidative metabolism.

1.4 The paradoxical role of PGC1α in cancer

As a central regulator of energy metabolism, PGC1α plays an important role in carcinogenesis and progression [16]. In multiple cancers, increased expression and activity of PGC1α is closely associated with the metabolic phenotype and facilitates tumor cell growth, invasion, distal dissemination and chemoresistance [17]. In melanoma, expression levels of PGC1α are tightly associated with the metabolism, biology and drug sensitivity. PGC1α positive melanoma cells exhibit increased mitochondrial capacity and survival under oxidative stress conditions [18]. In colorectal tumors,

chemotherapy induces a SIRT1/PGC1α dependent increase in OXPHOS and mitochondrial biogenesis that favor tumor survival during treatment [19]. Moreover, in human invasive breast cancers, clinical analysis revealed a strong positive correlation between PGC1α expression and the formation of distant metastases [20]. PGC1α interacts with a number of transcription factors and nuclear receptors, including NRF 1, ERRα (estrogen related receptor), YY1 and MEF2C, to increase mitochondrial OXPHOS function under high energy need condition [21]. In response to oncogenic signals, PGC1α/ERRα can be recruited to the promoter of genes involved in the TCA cycle and OXPHOS to initiate transcriptional programs, and this could favor pro neoplastic outcomes [16]. In breast cancer cells, the PGC1α/ERRα axis has been demonstrated to upregulate most of the genes involved in lactate metabolis [22]. Whereas the activation of PGC1α/ERRα axis may increase and utilize lactate as an alternative carbon source to favor the survival of cancer cells and this could confer resistance of tumors to treatment with PI3K/mTOR inhibitor [22]. Addition to promoting mitochondrial biogenesis and OXPHOS, PGC1α has been shown to drive mitochondrial β oxidation to maintain energy balance during increased energy demand and help protect mitochondria from the toxic lipid overload [23, 24, 25]. These factors could be beneficial for PGC1α's pro neoplastic effects. Although the main body of documents supports pro tumorigenic activity of PGC1α, paradoxical antineoplastic effects also exist for some tumor types [26, 27]. In VHL deficient clear cell renal cell carcinoma (ccRCC), elevated mitochondrial activity induced by PGC1α is tightly associated with increased ROS production, leading to augmented oxidative stress [26]. Similarly, in human cells and mouse models of intestinal cancer, PGC1α regulates enterocyte cell fate and protects against tumorigenesis by promoting mitochondrial mediated apoptosis through reactive oxygen species (ROS) accumulation [28]. Hence, all these findings indicate that the role of PGC1α in cancer cell fate determination is not univocal. The elegant function of PGC1α depends on the specific tumor context and tumor subpopulation with a particular metabolic phenotype [16] (Figure 4).

2. Mitochondria dysfunction

Mitochondria are the double membrane, cytoplasmic organelles which contain their self-replicating genome. Mitochondria perform key biochemical functions essential for metabolic homeostasis and are arbiters of cell death and survival [29]. Mitochondrial dysfunction is defined as diminished mitochondrial biogenesis, altered membrane potential, and the decrease in mitochondrial number and altered activities of oxidative proteins due to the accumulation of ROS in cells and tissues [30]. Indeed, mitochondria are the most important source of ROS in most of the mammalian cells [31]. ROS produced in mitochondria during OXPHOS process primarily triggered mitochondrial dysfunction by interacting with mitochondrial and cellular components such as DNA, proteins, lipids, and other molecules [30]. Mitochondrial specificity of superoxide scavenging is subject to membrane potential. Mitochondrial membrane potential (MMP) is a key indicator of mitochondrial activity, because it reflects the process of electron transport and oxidative phosphorylation, the driving force behind ATP production [32] (Figure 5).

3. Mitochondria in ferroptosis

Mitochondria play a pivotal role in metabolic plasticity in malignant cells, as well as in the regulation of many RCD processes [33]. Mitochondria seem to be involved in ferroptosis induced by cystine deprivation (CDI) which, indeed, is associated with mitochondrial membrane hyperpolarization and lipid peroxide accumulation [34] (Figure 6). Erastin treatment boosts the production of mitoROS which, in turn, cause opening of mitochondrial permeability transition pore (mPTP), dissipation of $\Delta\Psi m$ and ATP depletion [35, 36]. Mitochondrial ROS play a momentous role in regulated cell death. The model of glutamate-induced cell death, increased mitochondrial ROS generation acted as an important contributing factor [37]. Another researches suggested that ferroptosis induced by erastin and analogues leading to increased mitochondrial and cytosolic ROS generation, both mitochondrial targeted antioxidant MitoQ and ROS scavenger N-acetylcysteine (NAC) blocked mitochondrial and cytosolic production of ROS and rescued mitochondrial function and cell viability [38]. Mitochondria play a central role in fatty-acid metabolism and provide the specific lipid precursor for lipid oxidation. The

initial lipid peroxidation step generated in extra-mitochondrial compartments and this oxidation signals preceded mitochondrial lipid oxidation and cell lysis [39]. Also, mitochondrial lipid peroxidation seems to be a hallmark of ferroptosis. Cells undergoing ferroptosis exhibit mitochondria fragmentation and specific changes in mitochondrial morphology such as reduction of mitochondrial cristae and decrease in mitochondrial size [40]. Mitochondrial free iron accumulation exacerbates erastin-mediated ferroptosis [41]. Since mitochondrial iron metabolism mainly occurs in the mitochondrial matrix, iron must cross both the OMM and IMM. Iron transport across the IMM is an active process dependent on the membrane transporter mitoferrin 1 (Mfrn1) and its homolog mitoferrin 2 (Mfrn2). Dysregulation of Mfrn1/2 leads to mitochondrial iron accumulation and oxidative damage [42]. Squestering iron within mitochondria via overexpression of mitochondrial ferritin (FtMt) can counteract erastin-induced cell death [15]. These studies indicated that mitochondria damage may be the terminal process of ferroptosis.

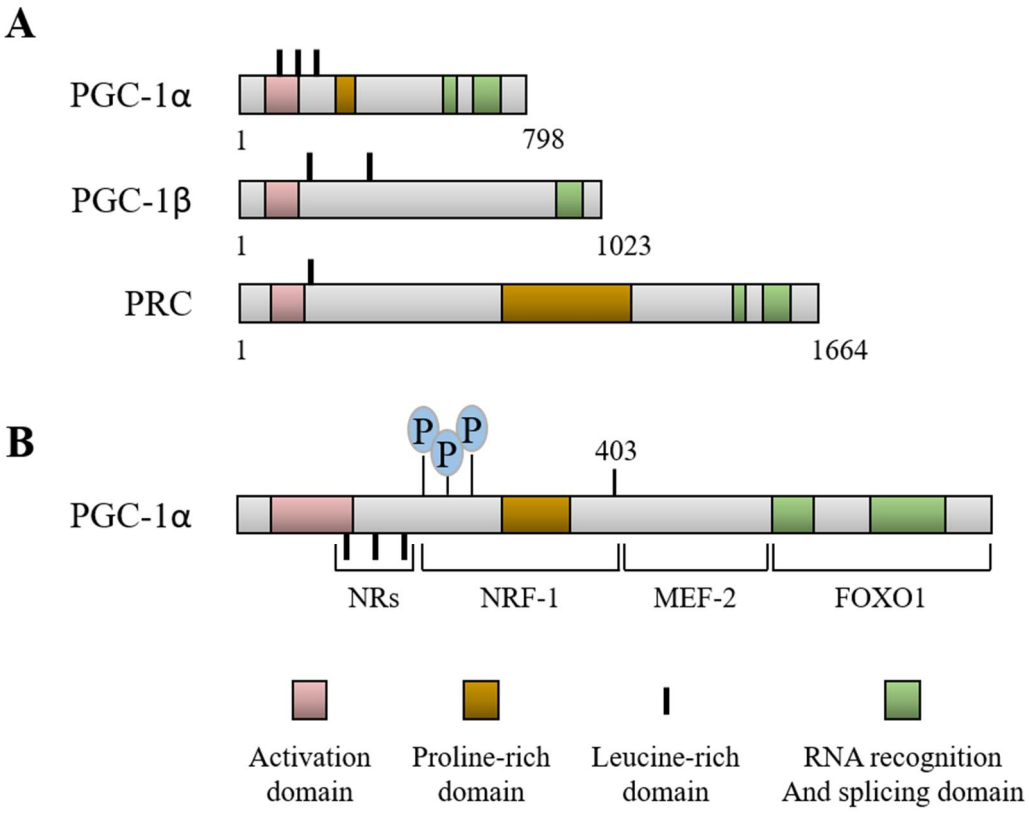

Figure 1. The PGC1 coactivator family: inducible boosters of gene transcription.

(A) The schematic depicts the relative length and shared domains of the 3 members of the PGC1 coactivator family. The nature of the domains is indicated in the key. (B) A schematic of the PGC1α molecule is shown to denote several key functional domains involved in the interaction with specific target transcription factors including NRs, nuclear respiratory factor-1 (NRF-1), MEF-2, and FOXO1. MAPK phosphorylation (P) sites are also shown. This figure was modified from *J Clin Invest*. 2006;116(3):615-622.

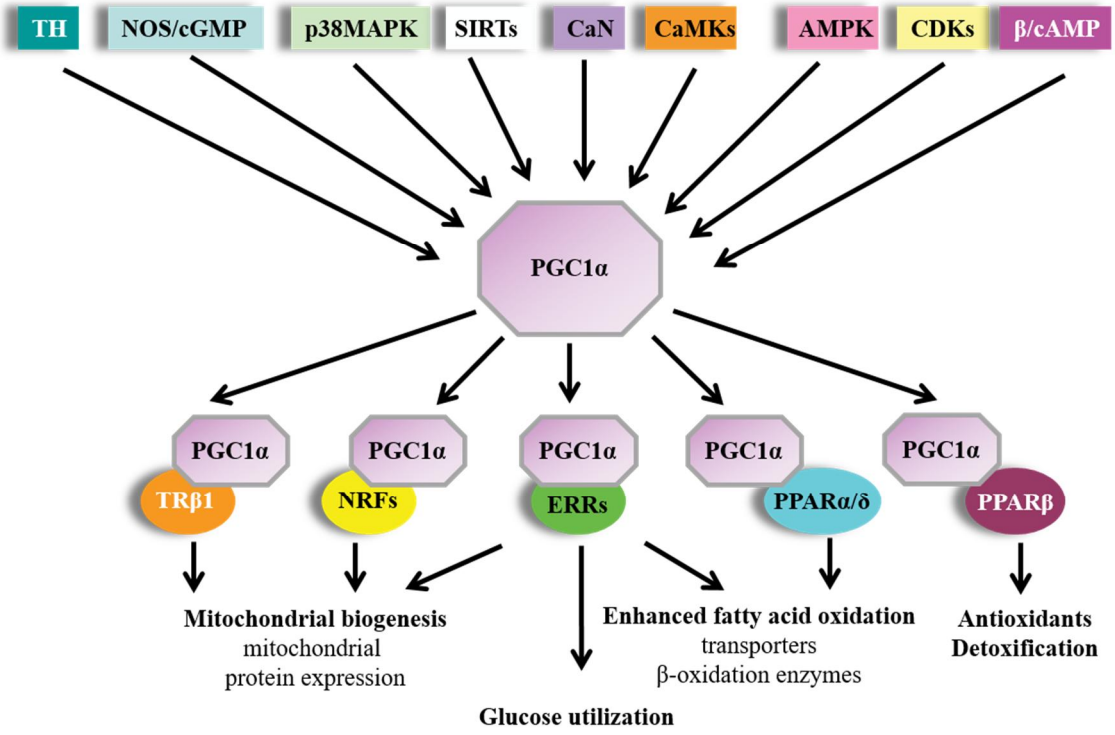

Figure 2. PGC1α regulatory cascade.

Thyroid hormone (TH), nitric oxide synthase (NOS/cGMP), p38 mitogen-activated protein kinase (p38MAPK), sirtuines (SIRTs), calcineurin, calcium-calmodulin-activated kinases (CaMKs), adenosine-monophosphate-activated kinase (AMPK), cyclin-dependent kinases (CDKs), and b-adrenergic stimulation (b/cAMP) have been shown to regulate expression and/or activity of PGC1α. PGC1α then co-activates transcription factors such as nuclear respiratory factors (NRFs), estrogen-related receptors (ERRs), and PPARs, known to regulate different aspects of energy metabolism including mitochondrial biogenesis, fatty acid oxidation, and antioxidant. This figure was modified from *Cardiovasc Res*. 2008 Jul 15;79(2):208-217.

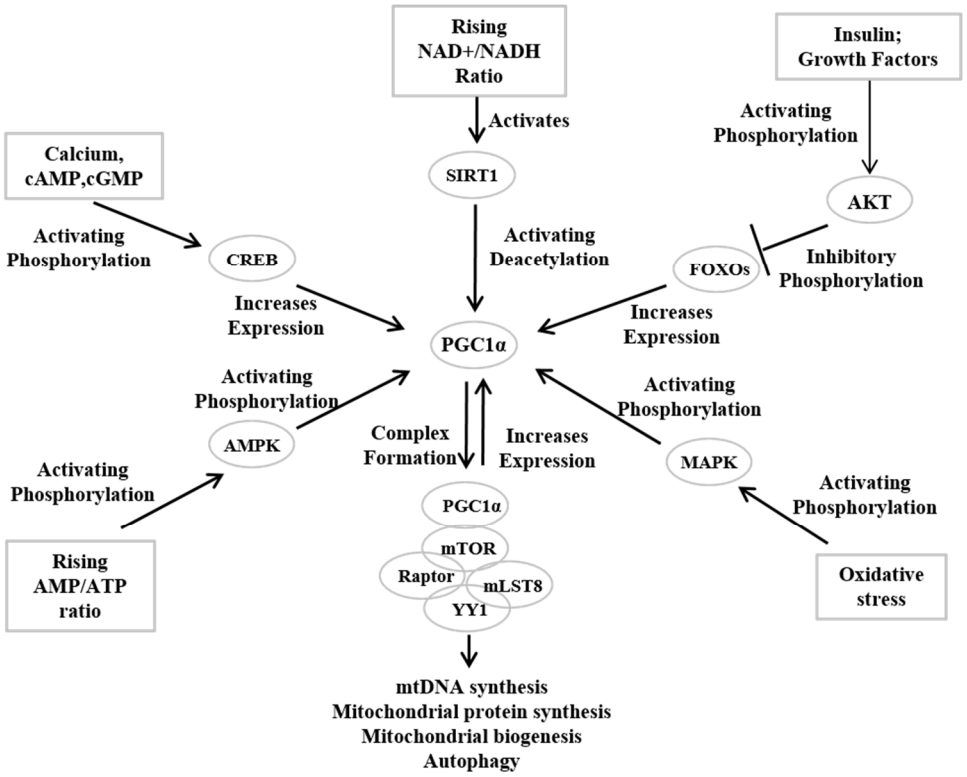

Figure 3. PGC1α is regulated by various nutrient, energy, and stress-sensing pathways

This diagram presents a schematic summary of different proteins and transcription factors that regulate PGC1α activity and levels. It is very simplified, and as more is learned about mitochondrial biogenesis the indicated relationships may change. Briefly, SIRT1-mediated PGC1α deacetylation and MAPK-mediated PGC1α phosphorylation induce PGC1α activation. AMPK also activates PGC1α through a direct phosphorylation event or indirectly through intermediates. The CREB transcription factor activates PGC1α expression. A FOXO transcription factor, FKHR, also appears to activate PGC1α expression; by retaining FOXOs in the cytosol, AKT phosphorylation of FOXOs would prevent this contribution. Activated PGC1α reportedly forms a super-complex with the mTOR-containing TORC1 complex (mTOR, raptor, and mLST8) and the YY1 transcription factor. This activated super-complex expresses genes needed to replicate mtDNA, produce mitochondrial proteins, accomplish mitochondrial biogenesis, and support autophagy. It also leads to the production of more PGC1α. This figure was modified from *Curr Pharm Des*. 2011;17(31):3356-3373.

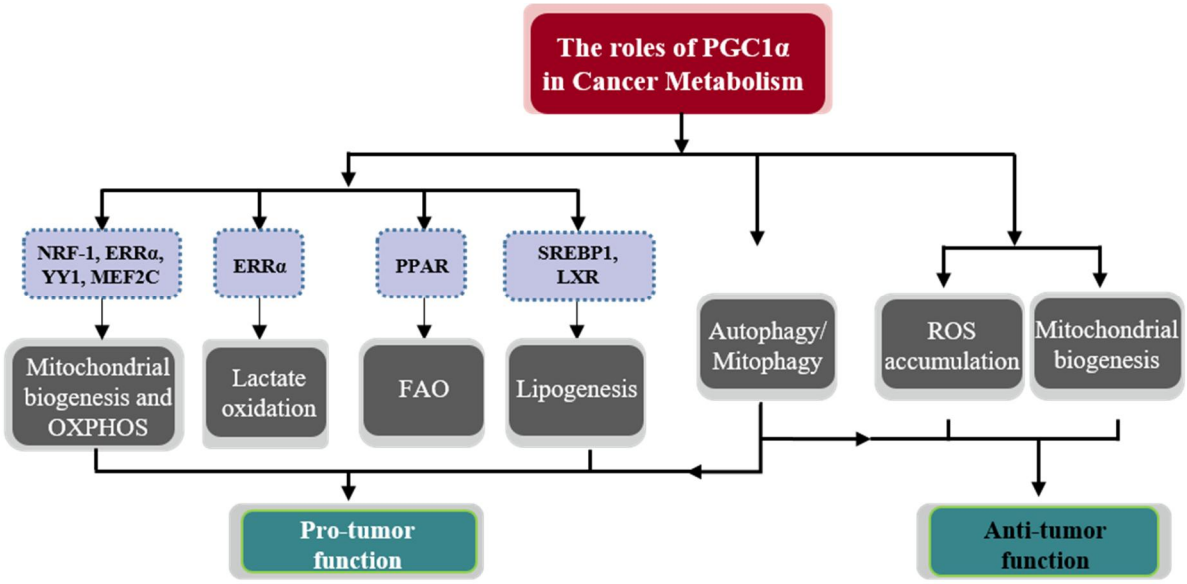

Figure 4. Role of PGC1α in the regulation of cancer metabolism.

The main altered metabolic pathways regulated by PGC1α and accounted for its pro□ and anti□tumor aspects in cancer cells. The pro□tumor effect of PGC1α mainly depends upon its ability to promote mitochondrial content and function, including mitochondrial biogenesis, mitochondrial respiration and fatty acid utilization. Although the main body of documents supports pro□tumorigenic activity of PGC1α, paradoxical antineoplastic effects also exist for some tumor types. This figure was modified from *Int J Cancer*. 2019 Sep 15;145(6):1475-1483.

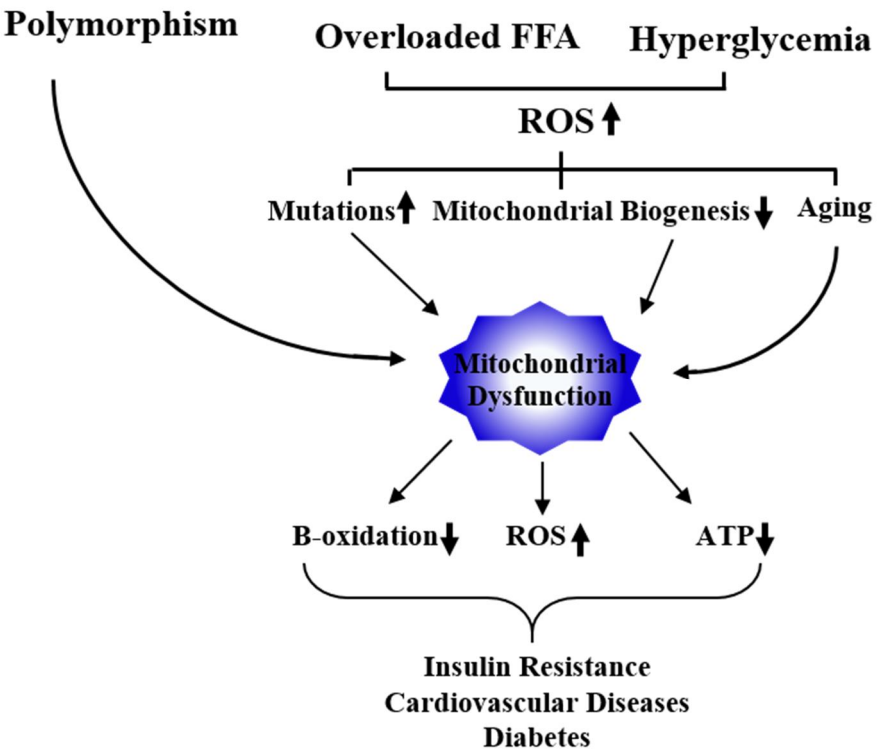

Figure 5. Mechanism of mitochondrial dysfunction.

Excess intake of nutrients, including overloaded FFAs or hyperglycemia conditions, increases ROS production and reduces mitochondrial biogenesis, causing mitochondrial dysfunction. Mitochondrial dysfunction leads to decreased β-oxidation and ATP production and increased ROS production, resulting in insulin resistance, diabetes, and cardiovascular disease. This figure was modified from *Circ Res*. 2008 Feb 29;102(4):401-414.

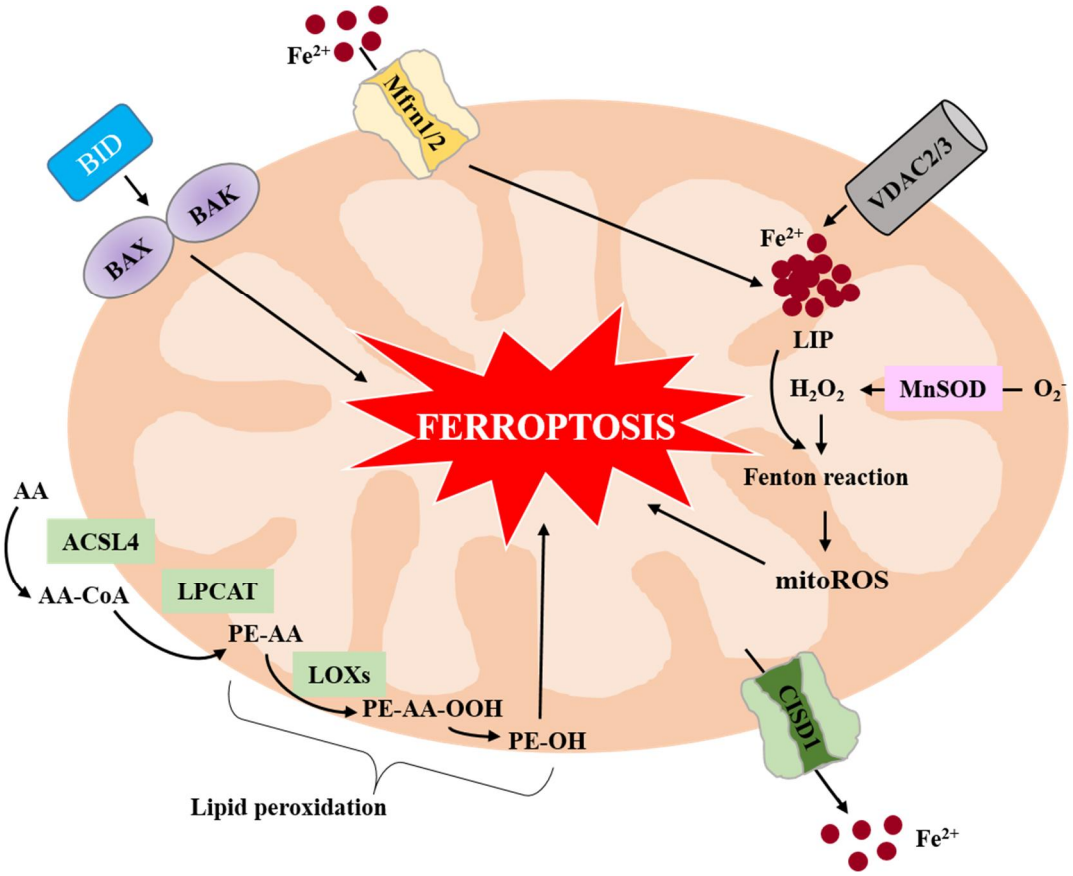

Figure 6. Mitochondrial metabolic processes in ferroptosis.

Iron uptake via Mfrn1/2 increases LIP amount, promoting mitoROS generation through Fenton Reaction. BID triggers ferroptosis through BAX and BAK activation and the consequent dysregulation of ΔΨm. VDAC2/3 imports $Fe2^{+}$ into mitochondria. Fe^{2+} contributes to enhance LIP which, in turn, generates mitoROS. MnSOD converts superoxide anion (O_2^-) from ETC to hydrogen peroxide (H_2O_2) which takes part into Fenton Reaction, thus promoting ferroptosis. CISD1 regulates mitochondrial iron export acting as ferroptosis suppressor. This figure was modified from *Cells*. 2020 Jun 20;9(6):1505.

Results

Erastin-induced cell death was decreased by PGC1α inhibitor, SR18292, in fibroblastic cells.

Mitochondria play a key role in iron metabolism, as well as substance and energy metabolism as it's the major organelle in iron utilization, catabolic and anabolic pathways [43]. PGC1α is also involved in mitochondrial biogenesis that is vital for cell survival [44]. To investigate the role of PGC1α in erastin-induced ferroptotic cell death, HT1080 cells were treated with vehicle or erastin (10μM) and total protein was harvested at the indicated times (0, 2, 4, 6, 8 and 10 hours). The levels of PGC1α protein began to increase by 4 hours, upon treatment with erastin (10μM), compared with treatment with vehicle (Figure 1A). Next, to determine the role of PGC1α in erastin-triggered cell death, cell viability was confirmed whether the PGC1α inhibitor, SR18292, affected erastin-induced cell death in HT1080 cells and MEF cells, respectively. As shown in Figure 1B and 1D, the erastin-induced cell death recovered in the presence of PGC1α inhibitor, SR18292 (20μM), compared with erastin treatment alone. Also, HT1080 cells and MEF cells treated with vehicle or erastin (10μM) in the absence or presence of PGC1α inhibitor, SR18292 (20μM) was confirmed cell cytotoxicity using lactate dehydrogenase (LDH)-release assay. The protective effects of PGC1α inhibitor, SR18292, still existed when the concentration of erastin (10μM) was caused loss of cell cytotoxicity without treatment with SR18292 (20μM) (Figure 1C and 1E). Taken together, these results suggested that PGC1α inhibitor, SR18292, potently protects form erastin-induced cell death in HT1080 cells.

Erastin-induced cell death was inhibited by PGC1α shRNA

HT1080 cells were transfected with PGC1α shRNA or control shRNA to investigate the effects of PGC1α expression under erastin-treated condition. To check down regulation of PGC1α expression in PGC1α shRNA transfected HT1080 cells, compared with control shRNA transfected HT1080 cells. Total protein and RNA were harvested and PGC1α levels were analyzed PGC1α shRNA or control shRNA transfected HT1080 cells. Protein and mRNA levels of PGC1α were decreased in PGC1α shRNA transfected HT1080 cells compared with control shRNA transfected HT1080 cells (Figure 2A and 2B). To further investigate the critical role of PGC1α, the cell viability was analyzed in response to erastin (10μM) in PGC1α shRNA transfected HT1080 cells compared with control shRNA transfected HT1080 cells. The viability of PGC1α shRNA transfected HT1080 cells was enhanced in presence of erastin, compared with that of control shRNA transfected HT1080 cells treated with erastin (Figure 2C). And then, PGC1α shRNA or control shRNA transfected HT1080 cells treated with vehicle or erastin (10μM) was confirmed cell cytotoxicity using lactate dehydrogenase (LDH)-release assay. The LDH release levels of PGC1α shRNA transfected HT1080 cells treated with erastin were decreased compared with that of control shRNA transfected HT1080 cells treated with erastin (Figure 2D). Therefore, the expression of PGC1α is an important mediator of erastin-triggered cell death, ferroptosis.

.

Erastin-induced lipid peroxidation and iron level were disrupted by down-regulated PGC1α.

Reactive oxygen species- (ROS-) induced lipid peroxidation plays a critical role in ferroptosis [45]. Thus, It was hypothesized that inhibition of PGC1α may contribute to the regulation of erastin-induced lipid peroxidation production in HT1080 cells. To investigate the role of PGC1α in erastin-induced lipid peroxidation, HT1080 cells were treated with vehicle or erastin (10μM) in the absence or presence of PGC1α inhibitor, SR18292 (20μM) and lipid peroxidation were assayed by flow cytometry using the fluorescent probes C11-BODIPY. As shown in Figure 3A, erastin treatment increased lipid peroxidation, compared with vehicle in HT1080 cells. Equally, PGC1α shRNA or control shRNA transfected HT1080 cells were treated with erastin (10μM) and lipid peroxidation were assayed by flow cytometry using the fluorescent probes C11-BODIPY. Erastin treatment increased lipid peroxidation compared with vehicle in control shRNA transfected HT1080 cells, but not in PGC1α shRNA transfected HT1080 cells (Figure 3B). The erastin-induced lipid peroxidation were disrupted upon inhibition of the PGC1α, compare with erastin treatment alone. Also, lipid peroxidation was examined by confocal imaging. Very low signals from oxidized BODIPY-C11 were detected under vehicle conditions, whereas its distribution shown by red fluorescence was mostly observed in intracellular compartments (Figure 3C, top panels). When HT1080 cells were treated with erastin (10μM) for 12 hours, oxidized signals gradually increased (Figure 3C, middle panels). In contrast, increased oxidized signals were almost blocked upon inhibition of the PGC1α, compare with erastin treatment alone (Figure 3C, lower panels). Ferroptosis is a novel defined form of regulated cell death, which is characterized by iron-dependent lipid peroxidation that ultimately leads to oxidative stress and cell death. Furthermore, iron is also an important component that composes a subunit of oxidase for lipid peroxidation. Therefore, the intracellular iron content was examined in HT1080 cells. Intracellular levels of ferrous ion were increased 6 hours after erastin (10μM) treatment. Furthermore, erastin-induced intracellular ferrous ion in HT1080 cells were found to decrease in the presence of the PGC1α inhibitor, SR18292 (20μM) (Figure 3D). Also, increased

intracellular ferrous ion levels in control shRNA transfected HT1080 cells with erastin were not seen in PGC1α shRNA transfected HT1080 cells treated with erastin. These results demonstrated that expression of PGC1α is an important mediator erastin-triggered lipid peroxidation and intracellular levels of ferrous ion.

Erastin-induced mitochondrial ROS was blocked in PGC1α inhibition.

PGC1α is a transcriptional coactivator that is a central inducer of mitochondrial biogenesis in cells [11]. PGC1α has a global effect on mitochondrial functions. To confirm whether erastin-induced ROS production is involved in mitochondrial ROS, cell viability was examined the impact of the mitochondria specific antioxidant, mito-TEMPO (10μM), on erastin-induced cell death in HT1080 cells. As shown in Figure 4A, erastin-induced cell death was recovered in the presence of mito-TEMPO compared with erastin treatment alone. To investigate the role of PGC1α in erastin-induced mitochondrial ROS, mitochondrial ROS were assayed for by flow cytometry using the fluorescent probes mitoSOX (mitochondrial ROS). MitoSOX fluorescence increased at 12 hours after erastin (10μM) treatment in HT1080 cells. The erastin-induced mitochondrial ROS were disrupted upon inhibition of the PGC1α by the SR18292 (20μM), compare with erastin treatment alone (Figure 4B). To determine whether the PGC1α knock down affected erastin-induced mitochondrial ROS, PGC1α shRNA or control shRNA transfected HT1080 cells were treated with erastin (10μM) and mitochondrial ROS were assayed by flow cytometry using the fluorescent probes mitoSOX. The mitochondrial ROS levels were increased after 12 hours of erastin in control shRNA transfected HT1080 cells. However, erastin-induced mitochondrial ROS levels were disrupted in PGC1α shRNA transfected HT1080 cells (Figure 4C). To determine whether erastin-induced ROS is also present in the cytosol, cytosolic ROS was measured by flow cytometry using the fluorescent probes CellROX® Deep Red. As shown in Figure 4D and 4E, cytosolic ROS levels of HT1080 cells, PGC1α shRNA and control shRNA transfected HT1080 cells did not increase in response to erastin (10μM) plus SR18292 (20μM) or erastin (10μM). These results suggested that erastin-induced ROS were mitochondria-specific.

Erastin-induced mitochondrial dependent ferroptosis was blocked in down-regulated PGC1α.

Erastin-induced mitochondrial dependent ferroptosis was blocked in down-regulated PGC1α Mitochondrial ferrous ion was increased in ferroptosis induced by erastin [43]. Mito-ferrin plays a key role in mitochondrial iron homeostasis as an iron transporter, importing ferrous iron from the intermembrane space of the mitochondria to the mitochondrial matrix [42]. Thus, protein expression levels of mito-ferrin were analyzed in HT1080 cells in response to vehicle or erastin (10μM) in the absence or presence of PGC1α inhibitor, SR18292 (20μM). Western blot revealed that protein levels of mito-ferrin decreased in erastin and SR18292 treated HT1080 cells, but not change erastin alone treated HT1080 cells (Figure 5A). In addition, mitochondrial lipid peroxidation was examined using the fluorescent probes MitoPeDPP by confocal imaging. When HT1080 cells were treated with erastin (10μM) for 12 hours, green fluorescence signals gradually increased (Figure 5B, middle panels), compared with vehicle (Figure 5B, top panels). In contrast, increased green fluorescence signals were almost blocked upon inhibition of the PGC1α, compare with erastin treatment alone (Figure 5B, lower panels). The levels of mitochondrial lipid peroxidation labeled with MitoPeDPP were also significantly increased after erastin (10μM) treatment in HT1080 cells. However, PGC1α inhibitor, SR18292 (20μM), significantly decreased mitochondrial lipid peroxidation levels.

Erastin-induced depolarization of mitochondrial membrane potential (MMP) was blocked by down-regulated PGC1α.

Erastin treatment boosts the production of mitoROS which, in turn, cause opening of mitochondrial permeability transition pore (mPTP), dissipation of ΔΨm and ATP depletion [35, 36]. To determine whether the PGC1α affected erastin-induced mitochondria dysfunction, mitochondria membrane potential was analyzed using fluorescent probes JC-1. HT1080 cells were treated with erastin (10μM) or erastin plus SR18292 (20μM) for 12 hours. Mitochondria membrane potential was assayed for by flow cytometry. Levels of mitochondria membrane potential were decreased 12 hours after erastin treatment in HT1080 cells. Loss of mitochondrial membrane potential by erastin significantly recovered in the presence of PGC1α inhibitor, SR18292 (Figure 6A). Also, PGC1α shRNA or control shRNA transfected HT1080 cells were treated with erastin (10μM) was confirmed mitochondrial membrane potential using fluorescent probes JC-1.Erastin treatment deceased mitochondria membrane potential compared with vehicle in control shRNA transfected HT1080 cells, but not in PGC1α shRNA transfected HT1080 cells (Figure 6B). Together, these results suggested that inhibition of PGC1α protects erastin-triggered mitochondria dysfunction.

Erastin-induced cell death was decreased expression in the presence of PGC1α inhibitor, SR18292.

Previously HO-1 was reported an essential enzyme for iron-dependent lipid peroxidation during ferroptotic cell death [46]. PGC1α is crucial for the induction of HO-1. Protein and mRNA levels of HO-1 were analyzed in HT1080 cells in response to erastin (10μM) in the absence or presence of PGC1α inhibitor, SR18292 (20μM) for the various time points. HT1080 cells treated with erastin (10μM) or erastin plus SR18292 (20μM). Erastin-induced HO-1 expression were decreased by PGC1α inhibitor, SR18292 (Figure 7A). Similarly, to the protein levels, the mRNA levels of HO-1 were dramatically diminished after erastin with SR18292 treatment (Figure 7B). Previously, it was known that erastin-induced ferroptosis was accelerated by the product of HO-1 [46]. To determined erastin-induced cell death, which is involved through down-regulation of HO-1 by the PGC1α inhibitor, the cell viability was measured using the HO-1 product. Hemin or CORM plus erastin treated cells were started to die much earlier than erastin alone. The effects of hemin (5μM) or CORM (10μM) were suppressed by cotreatment with PGC1α inhibitor, SR18292 (20 μM) (Figure 7C). These results demonstrated that HO-1, caused by erastin induced cell death, is regulated by PGC1α.

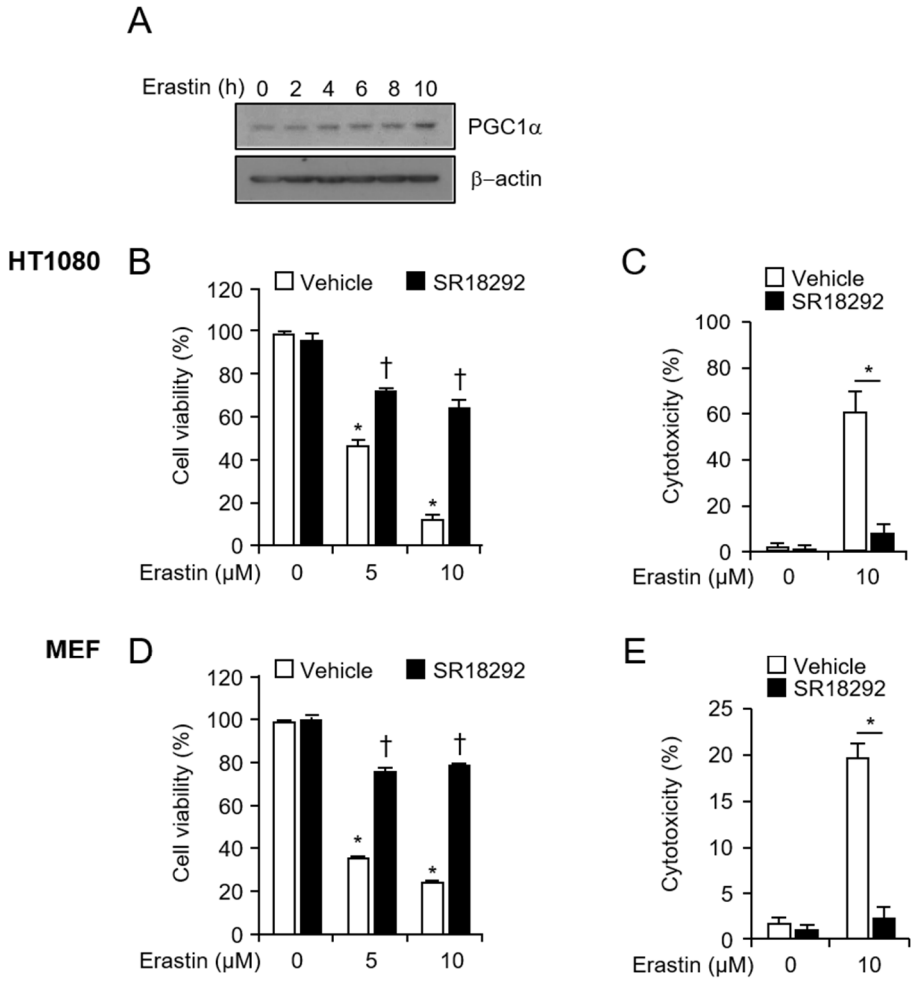

Figure 1. Erastin-induced cell death was decreased by PGC1α inhibitor, SR18292, in fibroblastic cells

HT1080 cells were treated erastin (10μM) for the indicated length of time points. PGC1α was assessed by Western blot analysis. β-actin was used as a loading control (A). The cell viability was analyzed in response to erastin (5, 10μM) or erastin plus SR18292 (20μM) in HT1080 cells (B), and WT MEF cells (D). *P < 0.05 indicates significant decrease compared with vehicle; †P < 0.05 indicates significant increase compared with erastin treatment. The cytotoxicity was analyzed in response to erastin (10μM) or erastin plus SR18292 (20μM) in HT1080 cells (C), and WT MEF cells (E) using LDH assay kit. Values are presented as mean ± SD, n=12. Experiments were performed at least three independent time. *P < 0.05 indicates significant decrease compared with erastin.

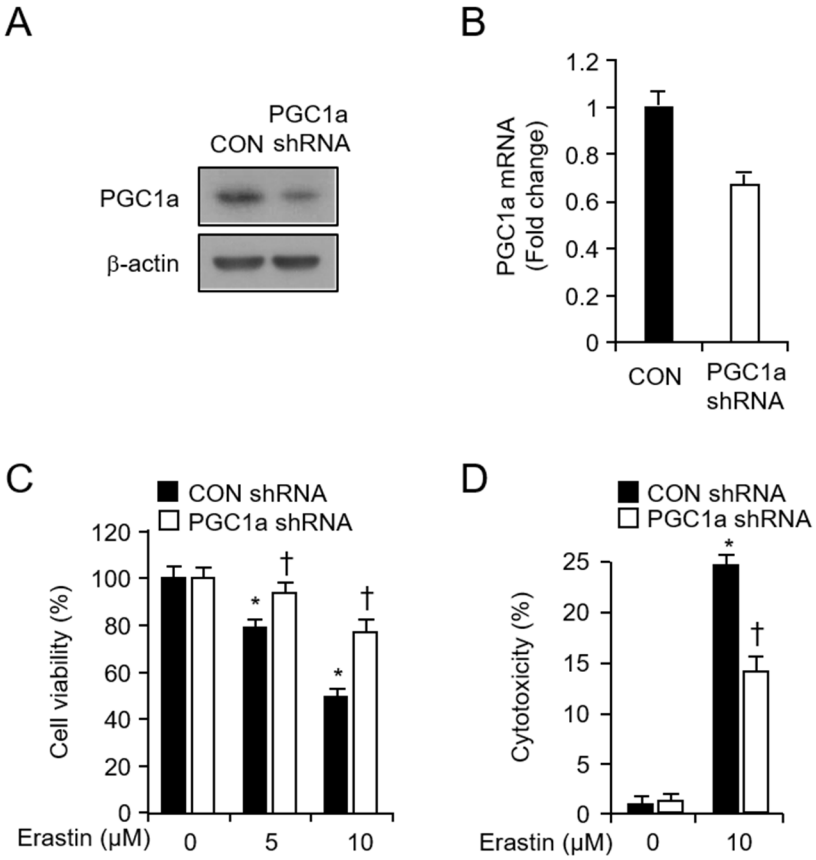

Figure 2. Erastin-induced cell death was inhibited by PGC1α shRNA

HT1080 cells were transfected with control or PGC1α shRNA. Protein levels (A) and mRNA levels (B) of PGC1α were analyzed to verify the downregulation of PGC1α expression. The cell viability was analyzed in response to erastin (5, 10μM) in HT1080 control or PGC1α shRNA transfected cells (C). *P < 0.05 indicates significant decrease compared with vehicle; †P < 0.05 indicates significant increase compared with erastin treatment. The cytotoxicity was analyzed in response to erastin (10μM) in HT1080 control or PGC1α shRNA transfected cells (D). *P < 0.05 indicates significant increase compared with control shRNA transfected cells; †P < 0.05 indicates significant decrease compared with erastin treatment in control shRNA transfected cells.

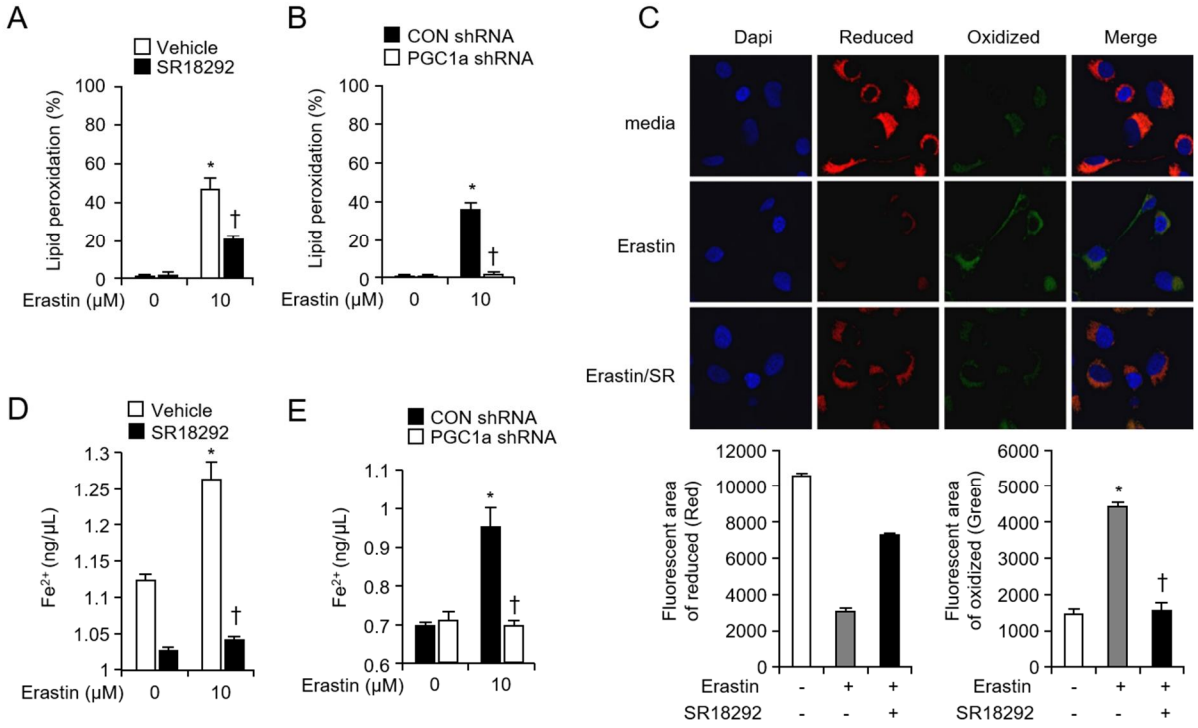

Figure 3. Erastin-induced lipid peroxidation and iron level were disrupted by down-regulated PGC1α.

The lipid peroxidation was analyzed in response to erastin (10μM) or erastin plus SR18292 (20μM) in HT1080 cells (A) using flow cytometry by the fluorescent probe C11-BODIPY. The lipid peroxidation was analyzed in response to erastin (10μM) in HT1080 control or PGC1α shRNA transfected cells using flow cytometry by the fluorescent probe C11-BODIPY (B). HT1080 cells were treated erastin (10μM) or erastin plus SR18292 (20μM) for 12 hours (C). Lipid peroxidation was assayed for by confocal microscope using the fluorescent probes C11-BODIPY. HT1080 cells (D) were treated with vehicle or erastin (10μM) in the absence or presence of SR18292 for 6 hours and intracellular iron levels were assessed using commercial assay kit. Intracellular iron levels were assessed 6 hours after erastin (10μM) in HT1080 control or PGC1α shRNA transfected cells (E). *P < 0.05 indicates significant increase compared with vehicle or control shRNA transfected cells; †P < 0.05 indicates significant increase compared with erastin treatment.

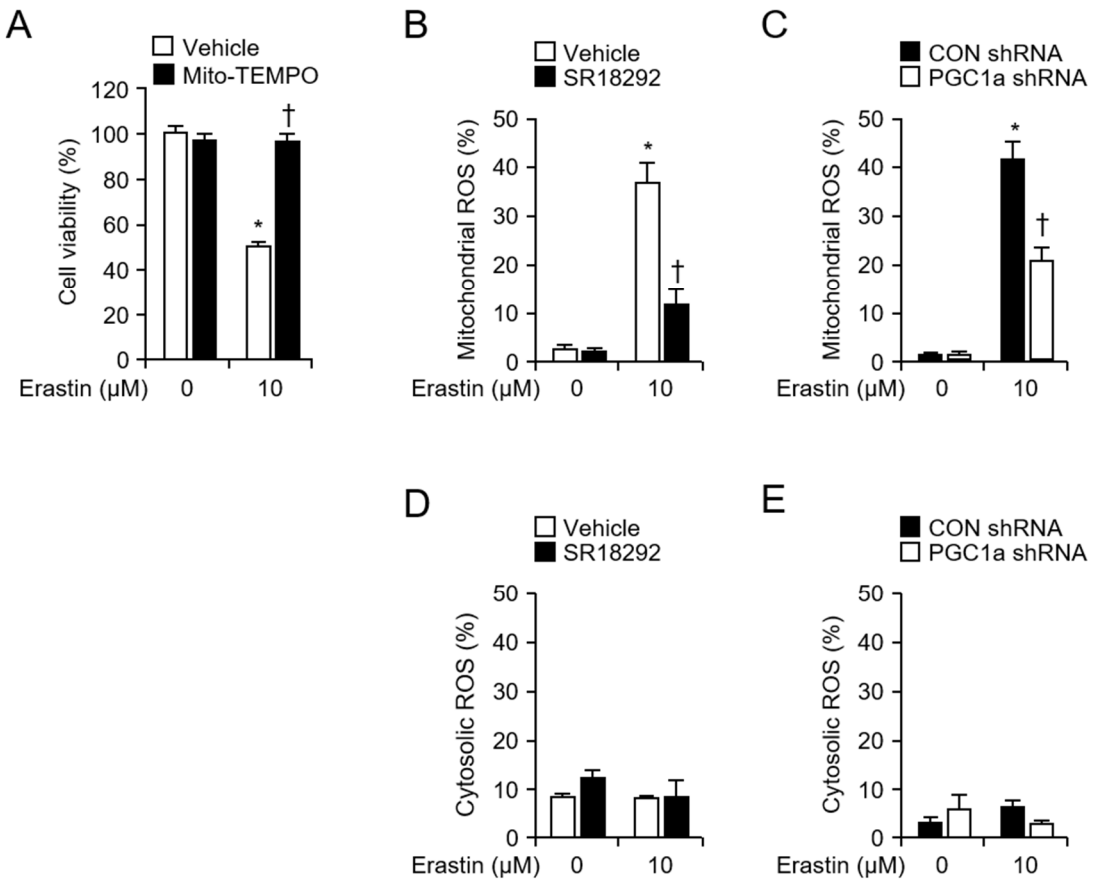

Figure 4. Erastin-induced mitochondrial ROS was blocked in PGC1α inhibition

The cell viability was analyzed 12 hours after erastin (10μM) or erastin plus mito-TEMPO (10μM) in HT1080 cells (A). *P < 0.05 indicates significant decrease compared with vehicle; †P < 0.05 indicates significant increase compared with erastin treatment. Mitochondrial ROS were assayed for by flow cytometry using the fluorescent probes mitoSOX. HT1080 cells were treated with erastin (10μM) or erastin plus SR18292 (20μM) for 12 hours (B). HT1080 control or PGC1α shRNA transfected cells were treated with erastin (10μM) for 12 hours (C). Cytosolic ROS were assayed for by flow cytometry using the fluorescent probes CellROX® Deep Red. HT1080 cells were treated with erastin (10μM) or erastin plus SR18292 (20μM) for 12 hours (D). HT1080 control or PGC1α shRNA transfected cells were treated with erastin (10μM) for 12 hours (E). *P < 0.05 indicates significant increase compared with vehicle or control shRNA transfected cells; †P < 0.05 indicates significant decrease compared with erastin treatment.

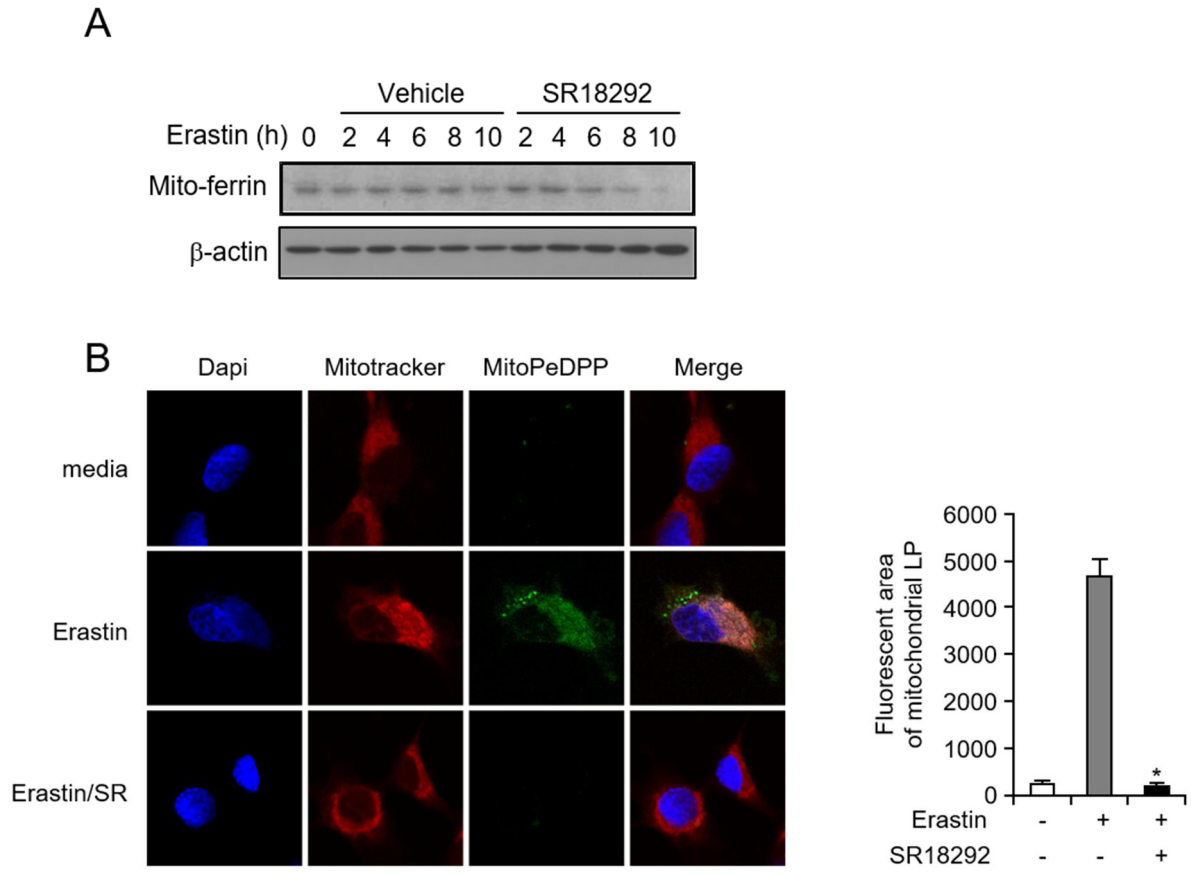

Figure 5. Erastin-induced mitochondrial dependent ferroptosis was blocked in down-regulated PGC1α.

HT1080 cells were treasted with erastin (10μM) or erastin plus SR18292 (20μM) for indicated time. Total protein was harvested and the protein levels of mito-ferrin were analyzed using western blot. β-actin was used as an internal loading control (D). HT1080 cells were treated erastin (10μM) or erastin plus SR18292 (20μM) for 12 hours (E). Mitochondria lipid peroxidation was assayed for by confocal microscope using the fluorescent probes MitoPeDPP. *$P < 0.05$ indicates significant decrease compared with erastin treatment.

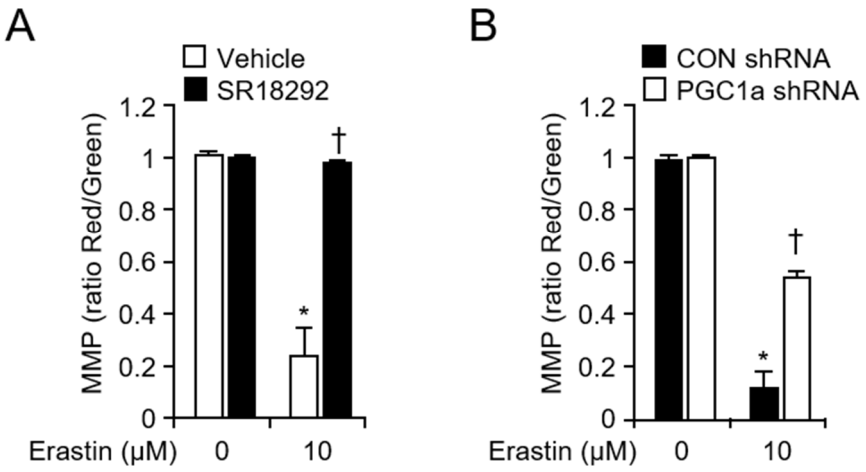

Figure 6. Erastin-induced depolarization of mitochondrial membrane potential (MMP) was blocked by down-regulated PGC1α.

Mitochondria membrane potential was assayed for by flow cytometry using the fluorescent probes JC-1. HT1080 cells were treated with erastin (10μM) or erastin plus SR18292 (20μM) for 12 hours (A). HT1080 control or PGC1α shRNA transfected cells were treated with erastin (10μM) for 12 hours (B). *P < 0.05 indicates significant decrease compared with vehicle and control shRNA transfected cells; †P < 0.05 indicates significant increase compared with erastin treatment.

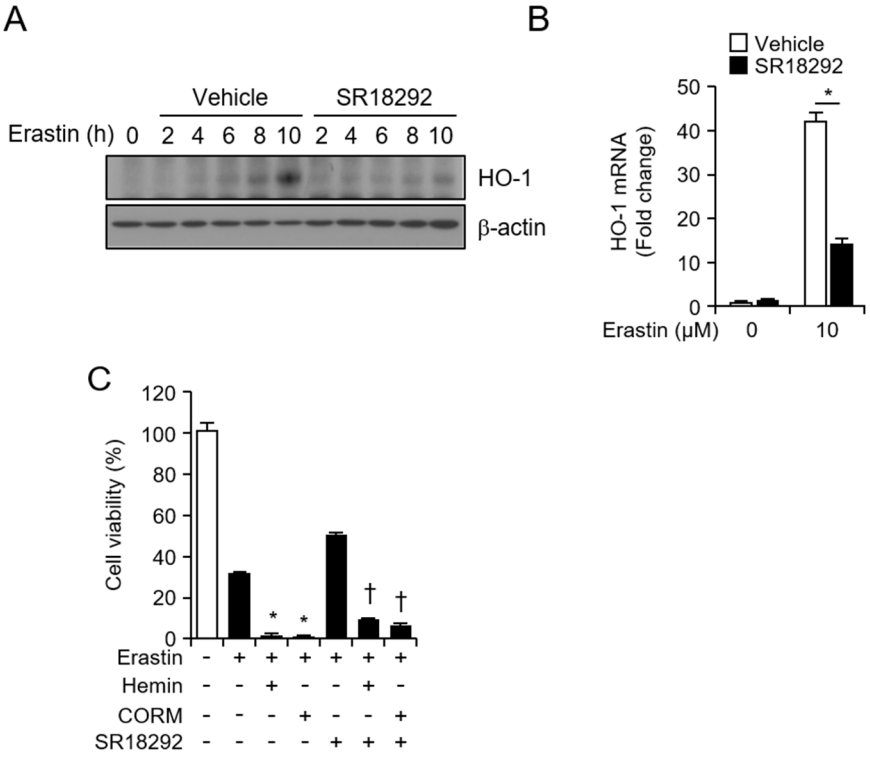

Figure 7. Erastin-induced cell death was decreased through down regulation of HO-1 expression in the presence of PGC1α inhibitor, SR18292.

HT1080 cells were treated with vehicle or erastin (10μM) in the absence or presence of PGC1α inhibitor, SR18292 (20μM) (A). Total protein was harvested and the protein levels of HO-1 were analyzed using western blot. β-actin was used as a loading control. Total RNA was extracted form HT1080 cells after erastin (10μM) in the absence or presence of PGC1α inhibitor, SR18292 (B). mRNA levels of HO-1 were analyzed by quantitative real-time RT-PCR. Human β-actin was used as a control for normalization. *P < 0.05 indicates significant decrease compared with erastin treatment; †P < 0.05 indicates significant increase compared with erastin treatment. Cell viability was analyzed 11 hours after vehicle, erastin (10μM), and Hemin (5μM) or CORM (10μM), plus erastin (10μM) and erastin, SR18292 and Hemin (5μM) or CORM (10μM) in HT-1080 cells. *P < 0.05 indicates significant decrease compared with erastin treatment; †P < 0.05 indicates significant increase compared with erastin plus Hemin or CORM treatment.

Discussion

Ferroptosis, an iron-dependent form of regulated necrosis, has emerged as a new cell death modality highly relevant to disease [47]. Ferroptotic cell death is morphologically, biochemically, and genetically distinct from apoptosis, various forms of necrosis, and autophagy. The phenomenon of ferroptosis is characterized by the overwhelming, iron-dependent accumulation of lethal lipid ROS, leading to lipid peroxidation in cancer cells [47]. Ferroptosis was primarily characterized by condensed mitochondrial membrane densities and smaller volume than normal mitochondria, as well as the diminished or vanished of mitochondria crista and outer membrane ruptured. Mitochondria play a role in iron metabolism, as well as substance and energy metabolism as it's the major organelle in iron utilization [43]. Interference of key regulators of mitochondrial lipid metabolism (e.g., ASCF2 and CS), iron homeostasis (e.g., ferritin, mitoferrin1/2 and NEET proteins), glutamine metabolism and other signaling pathways make a difference to ferroptotic sensitivity [43]. PGC1α has been implicated in mitochondrial biogenesis and increased mitochondrial respiration. The level of PGC1α expression is regulated in response to overstimulation, exemplifying the spectrum of situations to which mitochondrial biogenesis and activity must respond [5]. However, the role and effects of PGC1α in erastin-induced signaling pathways and cell viability have not been studied in HT1080 cells, yet. The goal of this study was to investigate the PGC1α involved in mechanism by which erastin induces HT1080 cell death and identify targets that can be used as a potential therapy. This research showed the expression and importance of PGC1α in erastin-induced ferroptotic cell death. And then, this study revealed that PGC1α inhibition protected HT1080 fibrosarcoma cells against erastin-induced cell death. As Figure 1 shown, PGC1α inhibitor, SR18292, prevents erastin-induced ferroptotic cell death, completely. Also, lipid peroxidation and intracellular iron levels were disrupted by PGC1α inhibitor, SR18292 (Figure 3). Similarly, the effects of HT1080 cell death were decreased in PGC1α shRNA transfected HT1080 cells in the presence

of erastin. These data suggest that functions and expression of PGC1α may important for erastin-induced cell death, ferroptosis in HT1080 cells. In addition, erastin treatment boosts the production of mitochondrial ROS [35, 36]. And, this study showed that inhibition of mitochondrial ROS by down-regulated of PGC1α protects HT1080 cells from erastin-induced cell death (Figure 4). In paradigms of programmed cell death, mitochondrial dysfunction is associated with the clash of the membrane potential and mitochondrial ROS production. Therefore, it was studied researched to confirm that ferroptosis could induce mitochondria dysfunction. PGC1α inhibitors interfered with erastin-induced mitochondrial dysfunction, such as loss of mitochondrial membrane potential (Figure 6). Mitochondrial ferrous ion was increased in ferroptosis induced by erastin [43]. Mito-ferrin plays a key role in mitochondrial iron homeostasis as an iron transporter, importing ferrous [42]. As Figure 5A shown, protein levels of mito-ferrin decreased in erastin and SR18292 treated HT1080 cells. In addition, mitochondrial lipid peroxidation significantly increased after erastin treatment in HT1080 cells. However, PGC1α inhibitor, SR18292, significantly decreased mitochondrial lipid peroxidation levels. Previously, HO-1 was suggested to serve a dominant role in ferroptosis [46]. The protein and mRNA levels of HO-1 were increased by erastin itself. Also, HO-1 may take part in iron supplement and lipid peroxidation in erastin-induced ferropotic cell death. PGC1α is crucial for the induction of HO-1. In this study, erastin-induced HO-1 expression were decreased by PGC1α inhibitor, SR18292. Similarly, to the protein levels, the mRNA levels of HO-1 were dramatically diminished after erastin with SR18292 treatment (Figure 7A and 7B). Moreover, Products of HO-1, Hemin or CORM, plus erastin treated cells were started to die much earlier than erastin alone. However, it was suppressed through down-regulated PGC1α. In this study, PGC1α, which affects ferroptosis, was shown to affect erastin-induced HO-1. Taken together, PGC1α is an essential for erastin-induced mitochondria dysfunction during ferroptotic cancer cell death.

Reference

1. Brian N. Finck and Daniel P. Kelly. PGC-1 coactivators: inducible regulators of energy metabolism in health and disease. *J Clin Invest*. 2006 Mar 1; 116(3): 615–622.

2. Puigserver, P., et al. A cold-inducible coactivator of nuclear receptors linked to adaptive thermogenesis. *Cell*. 1998. 92:829–839.

3. Lin J, Puigserver P, Donovan J, Tarr P, Spiegelman BM. Peroxisome proliferator-activated receptor γ coactivator 1β (PGC-1β), a novel PGC-1-related transcription coactivator associated with host cell factor. *J. Biol. Chem*. 2002; 277: 1645–1648.

4. Dankel SN, Hoang T, Flågeng MH, Sagen JV, Mellgren G. cAMP-mediated regulation of HNF-4alpha depends on the level of coactivator PGC-1alpha. *Biochim Biophys Acta*. 2010 Sep; 1803(9): 1013-1019.

5. Pablo J Fernandez-Marcos and Johan Auwerx. Regulation of PGC-1α, a nodal regulator of mitochondrial biogenesis. *Am J Clin Nutr*. 2011 Apr; 93(4): 884S–890S.

6. Zheqiong Tan, Xiangjian Luo, Lanbo Xiao, Min Tang, Ann M. Bode, Zigang Dong, and Ya Cao. The Role of PGC1α in Cancer Metabolism and its Therapeutic Implications. *Mol Cancer Ther*. 2016 May; 15(5):774-782.

7. Jager S, Handschin C, St-Pierre J, Spiegelman BM. AMP-activated protein kinase (AMPK) action in skeletal muscle via direct phosphorylation of PGC-1alpha. Proc Natl Acad Sci U S A 2007; 104: 12017–12022.

8. Rodgers JT, Lerin C, Haas W, Gygi SP, Spiegelman BM, Puigserver P. Nutrient control of glucose homeostasis through a complex of PGC-1alpha and SIRT1. Nature 2005; 434: 113–

118.

9. Knutti D, Kressler D, Kralli A. Regulation of the transcriptional coactivator PGC-1 via MAPK-sensitive interaction with a repressor. Proc Natl Acad Sci U S A 2001;98: 9713–9718.

10. Richard C Scarpulla. Metabolic control of mitochondrial biogenesis through the PGC-1 family regulatory network. *Biochim Biophys Acta*. 2011 Jul; 1813(7):1269-1278.

11. Shane Austin, Julie St-Pierre. PGC1α and mitochondrial metabolism – emerging concepts and relevance in ageing and neurodegenerative disorders. *Journal of Cell Science*. 2012 125: 4963-4971

12. Teng CT, Li Y, Stockton P, Foley J. Fasting induces the expression of PGC-1α and ERR isoforms in the outer stripe of the outer medulla (OSOM) of the mouse kidney. *PLoS One*. 2011; 6(11):e26961.

13. St–Pierre, J., Drori, S., Uldry, M., Silvaggi, J. M., Rhee, J., Jäger, S., Handschin, C., Zheng, K., Lin, J. and Yang, W. et al. Suppression of reactive oxygen species and neurodegeneration by the PGC-1 transcriptional coactivators. *Cell*. 2006. 127, 397–408.

14. St–Pierre, J., Lin, J., Krauss, S., Tarr, P. T., Yang, R., Newgard, C. B. and Spiegelman, B. M. Bioenergetic analysis of peroxisome proliferator-activated receptor gamma coactivators 1alpha and 1beta in muscle cells. *J. Biol. Chem*. 2003. 278, 26597–26603.

15. Valle, I., Alvarez–Barrientos, A., Arza, E., Lamas, S. and Monsalve, M. PGC-1alpha regulates the mitochondrial antioxidant defense system in vascular endothelial cells. *Cardiovasc. Res*. 2005. 66, 562–573.

16. Xiangjian Luo, Chaoliang Liao, Jing Quan, Can Cheng, Xu Zhao, Ann M. Bode, and Ya Cao. Posttranslational regulation of PGC 1α and its implication in cancer metabolism. *Int J Cancer*. 2019 Sep 15; 145(6): 1475–1483.

17. Frederic Bost and Lisa Kaminski. The metabolic modulator PGC-1α in cancer. *Am J Cancer Res*. 2019; 9(2): 198–211.

18. Vazquez F, Lim JH, Chim H, et al. PGC1α lpha expression defines a subset of human melanoma tumors with increased mitochondrial capacity and resistance to oxidative stress. *Cancer Cell*. 2013; 23: 287–301.

19. Vellinga TT, Borovski T, de Boer VC, et al. SIRT1/PGC1α lpha dependent increase in oxidative phosphorylation supports chemotherapy resistance of colon cancer. *Clin Cancer Res*. 2015; 21: 2870–2879.

20. LeBleu VS, O'Connell JT, Gonzalez Herrera KN, et al. PGC 1alpha mediates mitochondrial biogenesis and oxidative phosphorylation in cancer cells to promote metastasis. *Nat Cell Biol*. 2014;16: 992–1003.

21. Scarpulla RC. Metabolic control of mitochondrial biogenesis through the PGC 1 family regulatory network. *Biochim Biophys Acta*. 2011; 1813: 1269–1278.

22. Park S, Chang CY, Safi R, et al. ERRalpha regulated lactate metabolism contributes to resistance to targeted therapies in breast cancer. *Cell Rep*. 2016; 15: 323–335.

23. He F, Jin JQ, Qin QQ, et al. Resistin regulates fatty acid Beta oxidation by suppressing expression of peroxisome proliferator activator receptor gamma Coactivator 1alpha (PGC 1alpha). *Cell Physiol Biochem*. 2018; 46: 2165–2172.

24. Pambianco S, Giovarelli M, Perrotta C, et al. Reversal of defective mitochondrial biogenesis in limb girdle muscular dystrophy 2D by independent modulation of histone and PGC 1alpha acetylation. *Cell Rep*. 2016; 17: 3010–3023.

25. Jun HJ, Joshi Y, Patil Y, et al. NT PGC 1alpha activation attenuates high fat diet induced obesity by enhancing brown fat thermogenesis and adipose tissue oxidative metabolism.

Diabetes. 2014; 63: 3615–3625.

26. LaGory EL, Wu C, Taniguchi CM, et al. Suppression of PGC 1alpha is critical for reprogramming oxidative metabolism in renal cell carcinoma. *Cell Rep*. 2015; 12: 116–127.

27. Zhang Y, Ba Y, Liu C, et al. PGC 1alpha induces apoptosis in human epithelial ovarian cancer cells through a PPARgamma dependent pathway. *Cell Res*. 2007; 17: 363–373.

28. D'Errico I, Salvatore L, Murzilli S, et al. Peroxisome proliferator activated receptor coactivator 1 (PGC1-) is a metabolic regulator of intestinal epithelial cell fate. *Proc Natl Acad Sci.* USA 2011; 108: 6603–6608.

29. Paula I. Moreira, Xiongwei Zhu, Xinglong Wang, Hyoung-gon Lee, Akihiko Nunomura, Robert B. Petersen, George Perry, and Mark A. Smith. Mitochondria: A Therapeutic Target in Neurodegeneration. *Biochim Biophys Acta*. 2010 Jan; 1802(1): 212–220.

30. Jasvinder Singh Bhatti, Gurjit Kaur Bhatti, and P. Hemachandra Reddy. Mitochondrial dysfunction and oxidative stress in metabolic disorders - A Step towards mitochondria based therapeutic strategies. *Biochim Biophys Acta*. 2017 May; 1863(5): 1066–1077.

31. Daniel Munro, Jason R. Treberg. A radical shift in perspective: mitochondria as regulators of reactive oxygen species. *Journal of Experimental Biology*. 2017. 220: 1170-1180

32. Yi-Xuan Lee, Pei-Hsuan Lin, Endah Rahmawati, Yun-Yi Ma, Cindy Chan, Chii-Ruey Tzeng. Mitochondria Research in Human Reproduction. *The Ovary*. 2019. 3; 327-335

33. Paolo Ettore Porporato , Nicoletta Filigheddu , José Manuel Bravo-San Pedro, Guido Kroemer, Lorenzo Galluzzi. Mitochondrial metabolism and cancer. *Cell Res*. 2018 Mar;28(3): 265-280.

34. Anna Martina Battaglia, Roberta Chirillo, Ilenia Aversa, Alessandro Sacco, Francesco Costanzo, and Flavia Biamonte. Ferroptosis and Cancer: Mitochondria Meet the “Iron Maiden” Cell Death. *Cells*. 2020 Jun; 9(6): 1505.

35. Gao M., Yi J., Zhu J., Minikes A.M., Monian P., Thompson C.B., Jiang X. Role of mitochondria in ferroptosis. *Mol. Cell*. 2019; 73: 354–363.

36. Bernardi P., Di Lisa F. The mitochondrial permeability transition pore: Molecular nature and role as a target in cardioprotection. *J. Mol. Cell. Cardiol*. 2015; 78: 100–106.

37. S.A. Novgorodov, J.R. Voltin, M.A. Gooz, L. Li, J.J. Lemasters, T.I. Gudz. Acid sphingomyelinase promotes mitochondrial dysfunction due to glutamate-induced regulated necrosis. *J. Lipid Res*. 2018. 59. 312-329

38. .N. DeHart, D. Fang, K. Heslop, L. Li, J.J. Lemasters, E.N. Maldonado. Opening of voltage dependent anion channels promotes reactive oxygen species generation, mitochondrial dysfunction and cell death in cancer cells. *Biochem. Pharmacol*. 2018. 148 155-162

39. J.P. Friedmann Angeli, M. Schneider, B. Proneth, Y.Y. Tyurina, V.A. Tyurin, et al. Inactivation of the ferroptosis regulator Gpx4 triggers acute renal failure in mice. *Nat. Cell Biol*. 2014, 161180-161191

40. Lewerenz J., Ates G., Methner A., Conrad M., Maher P. Oxytosis/ferroptosis-(Re-) emerging roles for oxidative stress-dependent non-apoptotic cell death in diseases of the central nervous system. *Front. Neurosci*. 2018; 12: 214.

41. Strzyz P. Iron expulsion by exosomes drives ferroptosis resistance. *Nat. Rev. Mol. Cell Biol*. 2020; 21: 4–5.

42. Paradkar P.N., Zumbrennen K.B., Paw B.H., Ward D.M., Kaplan J. Regulation of mitochondrial iron import through differential turnover of mitoferrin 1 and mitoferrin. *Mol. Cell. Biol*. 2009; 29: 1007–1016.

43. Hai Wang, Can Liu, Yongxin Zhao, Ge Gao. Mitochondria regulation in ferroptosis. *Eur J Cell Biol*. 2020 Jan;99(1):151058.

44. Shang-Der Chen, Ding-I Yang, Tsu-Kung Lin, Fu-Zen Shaw, Chia-Wei Liou, Yao-Chung Chuang. Roles of oxidative stress, apoptosis, PGC-1α and mitochondrial biogenesis in cerebral ischemia. *Int J Mol Sci*. 2011;12(10): 7199-7215.

45. Lian-Jiu Su, Jia-Hao Zhang, Hernando Gomez, Raghavan Murugan, Xing Hong, Dongxue Xu, Fan Jiang, and Zhi-Yong Peng. Reactive Oxygen Species-Induced Lipid Peroxidation in Apoptosis, Autophagy, and Ferroptosis. *Oxid Med Cell Longev*. 2019; 2019: 5080843.

46. Min-Young Kwon, Eunhee Park, Seon-Jin Lee, Su Wol Chung. Heme oxygenase-1 accelerates erastin-induced ferroptotic cell death. *Oncotarget*. 2015 Sep 15;6 (27): 24393-24403.

47. Dixon SJ, Lemberg KM, Lamprecht MR, Skouta R, Zaitsev EM, Gleason CE, Patel DN, Bauer AJ, Cantley AM, Yang WS, Morrison B 3rd, Stockwell BR. Ferroptosis: an iron-dependent form of nonapoptotic cell death. *Cell*. 2012 May 25;149(5):1060-1

Material & Method

Reagents

Primary human dermal neonatal fibroblast (HDFn) and foreskin adult fibroblast (NuFF) cells were purchased from ATCC (Manassas, VA, USA). Erastin(329600) (EMD Millipore Corporation, USA), 3-methylaldehyde(M9281), Chloroquine (C6628), Bafilomycin A1 (B1793), N-acetyl-l-cysteine (A7250), mito-TEMPO (SML0737), DFO (D9533), ZLN005 (SML0802) (Sigma-Aldrich, St. Louis, MO, USA), SR18292 (HY-101491) (MedChemExpress, NJ 08852, USA) were purchased for reagents. Primary antibodies including anti-LC3B(L7943), anti-p62(P0067), anti-β-actin(A5441) (Sigma-Aldrich Co. LLC., St Louis, MO), anti-Beclin1(SC-11427), anti-TfR1(SC-9099), anti-PGC1α (SC-517380) (Santa Cruz Biotechnology, Inc., Santa Cruz, CA), anti-FTH1(4393S) (Cell Signaling Technology, Inc., Danvers, MA), anti-HO-1(SPA-896) (Enzo Life Sciences, Farmingdale, NY, USA), anti-mitoferrin(26469-1-AP) (Proteintech Group, Inc.) were used for western blotting analysis.

Cell culture

Primary pulmonary fibroblasts were isolated from $LC3B^{-/-}$, $BECN1^{+/-}$ mice and wild type littermates, as previously described. The lung tissue was soaked in a 1% antibiotic-antimycotic PBS (Invitrogen, Carlsbad, CA) twice for 20 min. The tissue was minced into 1-mm pieces, which were plated onto 100 mm dishes (30–40 pieces per plate). Fetal bovine serum was added dropwise over each tissue piece, and then the plates were incubated for 4 hours at 37°C. Then 2 mL of Dulbecco's modified Eagle's medium containing 10% fetal bovine serum and antibiotics was added to each plate. The plates were restored to the incubator and monitored every day until the fibroblasts reached confluence. Fibroblast cells were purchased from ATCC (Manassas, VA, USA), and cultured in DMEM medium (Gibco, Waltham, MA, USA) supplemented with 10% fetal bovine serum (Gibco, Waltham, MA, USA) and 1X Antibiotic-Antimycotic (100 U/mL penicillin, 100 μg/mL streptomycin, Fungizone® 0.25 μg/mL, Gibco,

Waltham, MA, USA) at 37°C in a humidified incubator with 5% CO_2. HT-1080 fibrosacoma cells were grown in RPMI 1640 medium (Life Technologies, Grand Island, NY) supplemented with 10% fetal bovine serum (Invitrogen, Life technologies, Carlsbad, CA), penicillin (100 u/mL), and streptomycin (100 μg/mL). All cells were incubated at 37°C in a humidified atmosphere of 5% CO2 and 95% air.

Cell viability assay

Cell viability was determined by the MTS assay using the CellTiter 96® AQueous One Solution Cell Proliferation Assay kit (Promega, Madison, WI). Cells were seeded at 0.7×10^4 cells per well in 96-well plates. After reagent treatment, 20 μl of MTS solution was added to each well. Plates were incubated for an additional 2~4 hours at 37°C. Absorbance at 490 nm was then measured using a SpectraMax M2 microplate reader (Molecular Devices, Sunnyvale, CA) to calculate the cell survival percentages.

Propidium Iodide (PI) staining assay

Cell death was analyzed by PI staining with flow cytometry. Fibroblast cells were seeded in 6-well plates at a density of 3×10^5 cells/well. For drug treatment experiments, we treated fibroblast with erastin 5uM and/or rapamycin (5 μM), 3-methylaldehyde (2 mM). After treat for 11 h, the cells were harvested, washed with phosphate-buffered saline (PBS), and stained with the Annexin V/ Propidium Iodide (PI) Apoptosis Detection Kit (Becton Dickinson, San Jose, CA, USA). Measurements were performed on a FACSCalibur (Becton Dickinson, San Jose, CA, USA) flow cytometer.

Construction of shRNA expressing HT1080 cells

PGC1α shRNA and nonspecific control shRNA (Sigma-Aldrich, St. Louis, MO, USA) were transfected into HT1080 cells using transfection reagents (#E2691) (Promega, Madison, WI) according to the protocol of the manufacturer. Briefly, for each transfection, shRNA (1 μg) was added to HT1080 cells for 24 hours, and stable clones expressing shRNA were further selected by puromycin (1.0 μg/mL). Cell culture medium containing puromycin was renewed every 48 hours, until resistant colonies could

be identified. The expression of PGC1α and the loading control (β-actin) in stable cells was tested.

Western blot analysis

The cells were harvested using RIPA buffer (Tris/Cl (pH 7.6); 100 mmole/L, EDTA; 5 mmole/L,NaCl; 50 mmole/L, β-glycerophosphate; 50 mmole/L, NaF; 50 mmole/L, Na3VO4; 0.1 mmole/L, NP-40; 0.5%, Sodium deoxycholate; 0.5%) with 1× Complete™ protease inhibitor Cocktail (#39922700) (Roche Applied Science, Mannheim, Germany). Protein concentrations of cell lysates were determined using the Pierce BCA protein assay kit (#23225) (Thermo Scientific, Rockford, IL). The samples were resolved with 12% sodium dodecyl sulfate–PAGE gels, and transferred to polyvinylidene difluoride (PVDF) membranes (Bio-Rad) overnight (120 mA). Membranes were blocked for 2 hours at room temperature with a 5% nonfat milk solution in TBST buffer (20 mM Tris–HCl, pH 7.4, 500 mM NaCl, 0.1% Tween 20). The blots were then incubated with various antibodies (diluted 1:1,000) in TBST overnight at room temperature. Equal loading was confirmed with an anti-β-actin (Sigma-Aldrich Co. LLC., St Louis, MO). The blots were then washed three times in TBST and incubated with an antirabbit secondary antibody or an anti-mouse secondary antibody in TBST for 1 hour at room temperature. Finally, immunoblots were detected by SuperSignal® West Pico Chemiluminescent Substrate (#34580) (Thermo Fisher Scientific, Inc., Waltham, MA) and visualized after exposure to X-ray film.

Iron assay

Levels of total iron were analyzed in wild type, $BECN1^{+/-}$, and $LC3B^{-/-}$ fibroblastic cells using the kit as described. An iron assay kit (Abcam, Cambridge, MA) was subsequently used to quantify total iron in the cell lysates according to manufacturer's instructions. Briefly, cells were harvested from a confluent T75 for each analysis. Cells can be lysed in 4 volume of iron assay buffer, centrifuge at 16000 x *g* for 10 min to remove insoluble materials. 5 µL iron reducer were added into 50 µl samples for total iron (Fe^{3+} plus Fe^{2+}) assay. Next, 100 µL iron probe solution was added into samples and incubated at 25°C for 60 min protected from light. Spectrophotometry was used to detect absorbance at 593 nm

wavelength.

Assessment of cytosolic ROS and Lipid peroxidation

Cells were seeded at 3×10^5 cells per well in 6-well plates. Next day, cells were treated with reagent for 12h. After 12h , cells were incubated with 2 mM CellROX® Deep Red (cytosolic ROS) or 2 μM C11-BODIPY581/591 (lipid peroxidation) (Invitrogen, Life Technologies, Grand Island, NY) for 30 min at 37°C in the dark. After 30 min of loading, unincorporated dye was removed by washings with 2% FBS containing PBS. Samples were then centrifuged at 1000 rpm for 3 min and the pellets were resuspended in 500 μL of 2% FBS containing PBS. Measurements were performed on a FACSCalibur (Becton Dickinson, San Jose, CA, USA) flow cytometer.

Confocal microscopy

HT1080 cells were grown on coverslips and treated with reagents for 12hours. After 12h , cells were incubated with 2 μM C11-BODIPY581/591 (lipid peroxidation) (Invitrogen, Life Technologies, Grand Island, NY) for 30 min at 37°C in the dark. And then, cells fixed for 20 min in 4% formaldehyde, rinsed 3 times in PBS. A nuclear counterstaining was made with a solution of 1 μg/mL Hoechst 33258 stain for 5 min and mounting on a slide using Fluorescence Mounting Medium (Dako). Olympus FV1000 MPE microscope was used to acquire images.

Assessment of Mitochondrial ROS formation

Formation of mitochondrial reactive oxygen species (ROS) was investigated via MitoSOX red staining (Invitrogen, Life Technologies, Grand Island, NY). For detection of mitochondrial ROS production, HT1080 cells were seeded in 6-well plates. After treatment with reagents, cells were stained with MitoSOX red for 30 min at 37 °C. After collecting and washing once with PBS, cells were re-suspended in PBS and red fluorescence was detected by FACS analysis. Data were collected from at least 10,000 cells.

Mitochondrial membrane potential

In order to determine changes in the MMP in HT1080 cells after reagents exposure, the MitoProbe™ JC-1 Assay Kit for Flow Cytometry (Invitrogen, Life Technologies, Grand Island, NY) was used. For detection of changes in MMP, HT1080 cells were seeded in 6-well plates. After treatment with reagents, cells were collected and stained with JC-1 at a final concentration of 2μM for 30 min at 37 °C. After washing with PBS cells were re-suspended in an appropriate amount of assay buffer and JC-1 fluorescence was assessed by FACS analysis. Data were collected from at least 10,000 cells.

LDH release assay

Cells were seeded at 0.7 × 104 cells per well in 96-well plates. After reagent treatment, the positive control was reconstituted with 100 μL LDH assay buffer. At the end of incubation, the plate was gently shaken to ensure LDH was evenly distributed in the medium. In the high control wells, 10 μL cell lysis solution was added, and the plate was shaken for 1 min and incubated at 37 °C for 30 min. Quantitative analysis was performed on the cell culture supernatant (5 μL/well). For each well, 95 μL of LDH Reaction Mix (LDH substrate mix, PicoProbe, LDH Assay Buffer) was added, bringing up the total volume to 100 μL/well. Absorbance was then measured at 450 nm using a SpectraMax M2 microplate reader (Molecular Devices, Sunnyvale, CA, USA) to calculate LDH release percentages.

Quantitative real-time reverse transcription-polymerase chain reaction (qRT-PCR)

For cultured cells, total RNA was isolated from cultured cells using TRIzol reagent (#15596018) (Thermo Fisher Scientific, Inc., Waltham, MA). Equal amounts of RNA were reverse transcribed with SuperScript™ III First-Strand Synthesis System (#18080-044) (Thermo Fisher Scientific, Inc., Waltham, MA) to cDNA. qRT-PCR was performed on the resulting cDNA using iQ SYBR Green Supermix (#170-8882AP) (Bio-Rad Laboratories, Inc., Hercules, CA). The comparative cycle threshold (Ct) value method, representing log transformation, was used to establish relative quantification of the fold changes in gene expression using StepOne plus system (Applied Biosystem, CA, USA). β-actin was used as an internal control (a commonly used loading control for gene degradation in PCR). Primers of human β-actin, HO-1 were purchased from Cosmo Genetech, Inc. (Seoul, Korea). The primers

sequences were as follows: human β-actin (forward: 5'-ATCGTGCGTGACATTAAGGAGAAG-3' and reverse: 5'-AGGAAGGAAGGCTGGAAGAGTG-3') human HO-1 (forward: 5'-TTCTCCGATGGGTCCTTACACT-3' and reverse: 5'- TCACATGGCATAAAGCCCTACA-3'). Amplification of cDNA started with 10 minutes at 95°C, followed by 40 cycles of 15 s at 95°C and 1 minute at 60°C.

Statistical analysis

All results were confirmed in at least three independent experiments; data from one representative experiment are shown. Quantitative data are shown as means ± standard deviation and significance of statistical analysis was determined with two-tailed, unpaired Student's *t*-test. *P*-values <0.05 were considered significant.

Ferroptotic 세포 사멸의 분자적 기전 연구

박은희

지도교수: 정 수 월

초록

프로그래밍 된 세포 사멸은 생물학 연구와 의학 분야 모두에서 각광받고 있는 주제이다. 그리고 표적 세포 사멸 과정은 암 치료의 일반적인 방법으로 알려져 있다. 그 중, Ferroptosis는 최근에 발견된 세포사멸의 한 종류로, 철(iron) 매개의 지질과산화(lipid peroxidation)에 의해 유도되는 세포사멸이다. 철은 산소 수송과 DNA 생합성 및 ATP 합성에 관여하는 인자로 세포 생존에 매우 중요한 역할을 한다. 철은 체내 포화지방산의 지질 과산화를 유도하며, 미토콘드리아에서 ATP 합성과 함께 활성산소(reactive oxygen species)를 생성한다. 이 과정에서 활성산소가 과하게 생성되면 산화적 스트레스(oxidative stress)가 증가하고 세포사멸이 일어나는데, 이를 ferroptosis라 한다. Ferroptosis의 형태학적 특징으로는 핵의 응축은 나타나지 않으며, 미토콘드리아의 크기가 수축하고 미토콘드리아의 외막 파열이 일어나고, 생화학적 특징으로는 세포 내 철의 양이 증가하고 지질 과산화의 축적이 나타난다고 보고되어 있다. 본 연구에서는 세포사멸의 또 다른 종류인 자가 포식(autophagy)와 ferroptosis의 상관관계와 그 과정에 관여하는 신호전달 분자들에 대한 메커니즘, 그리고 미토콘드리아 생합성과 산화적 대사 과정에서 중요한 역할을 하는 PGC1α가 ferroptosis에서 어떠한 역할을 하는지, 그 과정에 관여되는 분자 메커니즘에 대하여 알아보고자 하였다.

먼저, erastin에 의해 시작되는 ferroptotic 한 세포사멸에서 자가포식의 대표적 마커 유전자인 LC3B가 증가됨을 확인하였다. HT1080 세포에 LC3B shRNA 형질주입된 경우, erastin에 의해서 증가되었던 세포사멸의 수치가 감소되었다. 뿐만 아니라 자가포식의 활성제가 추가된 경우에는 세포사멸이 증가되었고, 억제제가 추가된 경우에는 감소됨을 볼 수 있었다. 또한, WT, Beclin1+/− 와 LC3B −/−의 섬유아세포를 이용하여 실험을 진행하였을 때, WT 섬유아세포에서 erastin에 의해 일어났던 세포사멸이

Beclin1+/− 와 LC3B −/−의 섬유아세포에서는 전혀 나타나지 않는 것을 볼 수 있었다. 그리고 WT, Beclin1+/− 와 LC3B −/−의 섬유아세포를 이용하여 페리틴의 저하와 transferrin 수용체의 유도에 의해 철에 의존적인 ferroptosis와 그에 의해 발생하는 autophagy를 확인하였다. 일관되게, autophagy의 결핍은 세포 내 철분의 고갈 및 지질 과산화를 감소시켜, erastin에 의한 ferroptosis에 의한 세포 사멸을 감소시킬 수 있었다는 점을 확인할 수 있었다. 또한, autophagy는 erastin에 의해 유도된 반응활성종(ROS)에 영향을 미쳤다. 이러한 결과들은 반응활성종에 의해 유도된 autophagy는 ferroptosis동안에 일어나게 되는 페리틴 분해와 transferrin 수용체 발현의 조절자로 작용하는 것을 시사한다.

둘째, erastin에 의해 시작되는 ferroptosis 세포사에서 PGC1α의 역할을 연구하였다. PGC1α는 대표적으로 미토콘드리아 생합성에서 중요한 역할을 한다고 알려져 있다. Erastin에 의해 ferroptosis가 일어날 때 PGC1α의 발현이 단백질 수준에서 증가됨을 확인하였고, PGC1α의 저해제로 알려진 SR18292가 ferroptotic한 세포사를 보호하는 것을 MTS와 LDH assay를 통해 확인할 수 있었다. 이러한 결과는 PGC1α shRNA가 형질주입된 HT1080 세포에서도 동일하게 결과를 볼 수 있었다. 뿐만 아니라, eratin에 의해 증가되었던 세포 내 철 수준과 지질 과산화의 수준이 PGC1α의 저해제인 SR18292을 함께 처리하게 하자 감소되는 것을 볼 수 있었고, PGC1α shRNA가 형질주입된 HT1080 세포에서도 마찬가지의 결과를 볼 수 있었다. 미토콘드리아 특이적 반응활성종 억제제인 mito−TEMPO를 통해서 erastin에 의해 증가되는 반응활성종이 미토콘드리아 특이적이라는 사실을 확인할 수 있었다. 또한, PGC1α는 erastin에 의해 증가되는 미토콘드리아 특이적 반응활성종(ROS)에 영향을 미쳤다. Mito−ferrin의 단백질 발현과 미토콘드리아 특이적 지질 과산화의 변화를 통해 erastin에 의해 증가되는 ferroptosis 세포사멸이 미토콘드리아 의존적임을 시사한다. 이는 결국 미토콘드리아의 역할에도 영향을 미치며 erastin에 의해 낮아졌던 미토콘드리아 막 전위가 PGC1α 억제제를 통해 복구됨을 볼 수 있었다. 마지막으로 이러한 결과들은 이미 앞서 발표되었던 HO−1에 의존적인 ferroptosis 세포사멸에 영향을 미칠것으로 보인다.

따라서, 본 연구에서 erastin에 의해 나타나는 ferrototosis 세포사멸에서 또 다른 세포사멸의 종류인 자가포식과의 관계, 미토콘드리아의 주요 분자, PGC1α와의 관계에 대하여 처음으로 규명하였다. 위의 연구는 암 치료에서 대표적으로 쓰이는 표적 세포 사멸

과정에 바탕이 되며 암 치료목적의 약물 개발에 도움이 될 것으로 생각된다.